

**Chasing the 400-kyr pacing of deep-marine sandy submarine fans: Middle Eocene
Aínsa Basin, Spanish Pyrenees**

Blanca Cantalejo ^{1*}, Kevin T. Pickering ¹, Ken G. Miller ², Conall Mac Niocaill ³

¹ Department of Earth Sciences, University College London (UCL), Gower Street, London, WC1E 6BT, U.K.

² Department of Earth and Planetary Sciences, Rutgers University, Piscataway, NJ 08854, U.S.A.

³ Department of Earth Sciences, University of Oxford, Oxford, OX1 3AN, U.K.

Email: ucfbca@ucl.ac.uk

Keywords: orbital tuning, gamma-ray, time-series, deep-marine, climatic, tectonic, Middle Eocene

Abstract

In an attempt to understand the relative importance of climate and tectonics in modulating coarse-grained sediment flux to a tectonically-active basin during what many researchers believe to be a greenhouse period, we have studied the Middle Eocene deep-marine Aínsa Basin, Spanish Pyrenees. We use orbital tuning of many spectral gamma-ray logged fine-grained siliciclastic sections, already shown to contain Milankovitch frequencies, in conjunction with a new high-resolution palaeomagnetic study through the basin sediments, to identify polarity reversals in the basin as anchor points to allow the conversion of a depth-stratigraphy to a chronostratigraphy. We use these data, in conjunction with a new age model incorporating new biostratigraphic data, to pace the development of the deep-marine sandy submarine fans over ~8 million years. Timing for the sandy submarine fans shows that, unlike for the fine-grained interfan sediments, coarse-grained delivery to the basin was more complex. Approximately 72% of the sandy fans are potentially coincident with the long-eccentricity (400-kyr) minima and, therefore, potentially recording changing climate. The stratigraphic position of some sandy fans is at variance with this, specifically those that likely coincide with a period of known increased tectonic activity within the Aínsa Basin, which we propose represents the time when the basin was converted into a thrust-top basin (Gavarnie

thrust sheet), presumably associated with rapid uplift and redeposition of coarse clastics into deep-marine environments. We also identify sub-Milankovitch climate signals such as the ~41.5 Ma Late Lutetian Thermal Maximum (LLTM). This study demonstrates the complex nature of drivers on deep-marine sandy fans in a tectonically-active basin over ~8 Myr. Findings of this study suggest that even during greenhouse periods, sandy submarine fans are more likely linked with times of eccentricity minima and climate change, broadly consistent with the concept of lowstand fans. However, hysteresis effects in orogenic processes of mountain uplift, erosion and delivery of coarse siliciclastics via fluvial systems to coastal (deltaic) and shallow-marine environments, likely contributed to the complex signals that we recognise, including the 2–3 Myr time gap between the onset of deep-marine fine-grained sediments in the early development of the Aínsa Basin and the arrival of the first sandy fans.

The principal processes that drive high-frequency modulation of sediment flux to deep-marine environments include climate change that may be associated with eustatic sea-level change, sediment flux via terrestrial drainage systems, tectonics, and autocyclicality.

Many researchers recognise a strong climatic/eustatic control for the deposition of sediment gravity flow (SGF) deposits and submarine-fan development in ocean basins, *e.g.*, for the Amazon Fan (Manley and Flood, 1988; Flood and Piper, 1997; Maslin *et al.*, 2006), Mississippi Fan (Bouma *et al.*, 1989; Feeley *et al.*, 1990; Weimer, 1990; Kolla and Perlmutter, 1993), Nile Fan (Maldonado and Stanley, 1976; Ducassou *et al.*, 2009), Bengal Fan (Weber *et al.*, 2003), Indus Fan (Kolla and Coumes, 1987; von Rad and Tahir, 1997, Prins *et al.*, 2000; Bourget *et al.*, 2013), Mozambique Fan (Marz *et al.*, 2008), the Zaire Fan (Babonneau *et al.*, 2002; Anka and Séranne, 2004), the Antarctic Pacific margin (Barker and Camerlenghi, 2002), and the glacially influenced, canyon-dominated Southwest Grand Banks Slope, Canada (Armitage *et al.*, 2010). Such climatic/eustatic control at a Milankovitch timescale has also been identified in ancient tectonically-active deep-marine basins, although during an icehouse period when large-amplitude eustatic sea-level change occurred (*e.g.*, the Kazusa Group forearc basin, SE Japan, by Pickering *et al.*, 1999; the Corinth rift, Greece, by Weltje and de Boer, 1993, and Backert *et al.* 2010). Some submarine fans show active growth during both rising sea level and highstands (Piper and Normark, 1983; Kuehl *et al.*, 1989; Flood *et al.*, 1991; Kolla and Perlmutter, 1993; Weber *et al.*, 1997; Covault *et al.*, 2007; Ducassou *et al.*, 2009; Covault and Graham, 2010).

During sea-level falls, deltas may prograde to the shelf-edge break, releasing large volumes of sediment on the slope or in to canyon heads, increasing sediment flux to the deep-sea (Damuth, *et al.*, 1988; Bouma *et al.*, 1989; Nelson *et al.*, 1992; Kenyon *et al.*, 1995; Normark *et al.*, 1997; von Rad and Tahir, 1997; Prins *et al.*, 2000; Ducassou *et al.*, 2009). The progressive exposure during sea-level lowstands typically corresponds to slope instability and the triggering of MTDs/MTCs. Thick intervals of sediment slides, slumps and debris flows (MTDs/MTCs) typically occur at the base of a deep-marine fan system (Ducassou *et al.*, 2009). However, although sea-level lowstands greatly favour the development of submarine fans, the timing and type of SGF events in these systems may depend not only on sea-level changes, and its rate of change, but also on the nature of available sediments, shelf and river processes in the staging area for SGFs, tectonic setting, and seafloor topography / gradients of the basins (*cf.* Kolla and Macurda, 1988; McHargue, 1991).

During warmer and wetter periods, increased river-water discharge may cause increased erosion of fluvial and older deposits (Blum and Tornqvist, 2000), resulting in increased sediment flux to the shelf margin. High fluvial discharge may result in the progradation of deltas to the shelf-edge and to deep-marine environments (Burgess and Hovius, 1998; Carvajal *et al.*, 2009). Burgess and Hovius (1998) proposed that in the absence of significant sea-level fluctuations, for instance during greenhouse conditions, fan growth can continue if rivers and deltas have sufficient sediment loads (flux) allowing sediment to be transported to the shelf edge. Ducassou *et al.* (2009) found that in the Nile submarine fan, periods of increased SGF activity and the accumulation of MTDs/MTCs occurred during phases of major flooding. During more arid periods, fluvial discharge decreased (Blum and Tornqvist, 2000), and sediments were temporarily stored within the drainage basin (fluvial deposits including alluvial fans).

Several studies have shown that tectonic processes may trigger submarine fan initiation. Periods of active thrusting could result in the creation of relief in the hinterland associated with an increased supply of coarse clastic sediment, whilst during tectonic quiescence, fine-grained deposition would dominate (de Boer *et al.*, 1991). Tectonic pulses of coarse-grained sediment have been invoked in Pleistocene successions, in pull-apart basin, SE Turkey (Dunne and Hempton, 1984), and in the northeastern Ebro basin, southeastern Spanish Pyrenees, (Guillocheau, 2010). Various studies that model tectonic processes suggest that fault activity can be intermittent and produce semi-cyclic depositional patterns at similar timescales to those of climatic processes (tens of thousands of years) (Peper *et al.*, 1992;

Peper and de Boer, 1995; Beekman *et al.*, 1995; Lee and Schwarcz, 1996; Nicol *et al.*, 1997, 2005; Morley *et al.*, 2000; Walsh *et al.*, 2002; Mouslopoulou *et al.*, 2009).

Autocyclic processes may also act to influence the distribution of submarine fan sediments. These processes include channel migration and avulsion, lobe switching and lateral compensational stacking patterns (Kenyon *et al.*, 1995; Parsons *et al.*, 2002; Nicholas and Quine, 2007; Deptuck *et al.*, 2008; Prélat *et al.*, 2010; Clarke *et al.*, 2010). Such processes occur because there is a tendency for sediment gravity flows to occupy topographic lows and smooth topographic relief (Mutti and Sonnino, 1981; Straub *et al.*, 2009; Ganti *et al.*, 2011). Cohesive flows, including MTDs/MTCs, however, can create mounded seafloor topography to create so-called "ponded" accommodation space where compensational stacking patterns and channel migration may occur (*e.g.*, Martinsen and Bakken, 1990; Ross *et al.*, 1994; Pickering and Corregidor, 2005). In the Danube submarine fan, where sea-level controlled fan activity, with the fan being most active during lower sea level, has been interpreted by Popescu *et al.* (2001) to show the development of the most recent channel-levée system during a single lowstand being influenced by channel avulsion and sand delivery under autocyclic processes.

From the above, it is clear that attempting to discriminate between the effects of the main drivers on sediment flux and deposition in deep time has proven challenging. Most studies that recognise a climatic origin focus on the strength or amplitudes of the orbital cycles, but not the phase relationship of climate response to orbital forcing, something that is important for understanding the forcing mechanism/s caused by global climate change. In addition, many basins around the world have complex and/or poorly understood tectonic evolution and non-unique sediment entry points that may result in complicated basin infills which adds complexity to the recognition of the main sediment drivers.

The deep-marine Aínsa Basin stratigraphy comprises a cyclic alternation of coarse-grained sandstone packages (interpreted as sandy submarine fans) and fine-grained packages of mostly fan lateral-margin, including levée, and interfan sediments (Pickering and Bayliss, 2009; Pickering and Cantalejo, 2015, and references therein). The presence of these sediment packages shows significant variation in sediment supply to the basin with alternating periods of coarser-grained and finer-grained sediments. Trying to understand the main driver on the deposition of the coarse-grained deep-marine submarine fans in the Aínsa Basin has proven controversial, with some researchers advocating a tectonic origin (Mutti, 1983-84; Muñoz *et*

al., 1994, 1998; Arbués *et al.*, 1998; Pickering and Corregidor, 2005; Moody *et al.* 2012; Castellort *et al.*, 2017) and others a climatic origin (Das Gupta and Pickering, 2008; Pickering and Bayliss, 2009; Sutcliffe and Pickering, 2009). In this study, we have investigated the main depositional drivers in the Aínsa Basin, Spanish Pyrenees.

Cantalejo and Pickering (2014, 2015), and Scotchman *et al.* (2015), analysed many fine-grained cyclostratigraphic sections in the Aínsa Basin using various geochemical proxies for environmental change, including outcrop spectral gamma-ray data in interfan and channel-levée-overbank successions throughout the entire deep-marine stratigraphy of the Aínsa Basin, and demonstrated a strong Milankovitch forcing with the short eccentricity and obliquity cycles appearing dominant in most of the records and precession cycles not always being present. These high-frequency variations in the supply of finer-grained sediments to the deep-marine Aínsa Basin were interpreted as due to changing storminess and continental runoff during warmer and wetter periods (Cantalejo and Pickering, 2014, 2015). The underlying driver on the increased flux of coarser-grained sands into the basin, however, remains unresolved and is the focus of this paper.

This study presents orbital tuning of mainly gamma-ray-logged fine-grained successions described in Cantalejo and Pickering (2014, 2015) and ties the stratigraphy to an age model of the basin constrained by new palaeomagnetic data, with the aim of establishing the precise timing of initiation of individual sandy submarine fans. By converting the stratigraphy of the Aínsa Basin into a chronostratigraphic framework, for the first time in any deep-marine sedimentary basin in deep time, we are better able to understand the likely underlying control/s on coarse-grained sediment delivery.

Our study aims to improve the understanding of controls on the timing of coarse-grained sediment supply within finer-grained cyclic sedimentation in tectonically-active basins, and to serve as a potential model for other studies in modern and ancient deep-marine basins worldwide.

Geological setting

The Aínsa Basin is amongst the best natural laboratories in which to study controls on siliciclastic, structurally-confined, deep-marine systems for several reasons: (i) a complete deep-marine basin stratigraphy with a duration of ~8–10 Myr; (ii) the principal sediment

source was from a single or several very closely-spaced entry point/s at the east/southeast end (present co-ordinates) of the basin; (iii) mapping shows that the sandy submarine fans were episodic with only one major submarine channel active at any time (Pickering and Bayliss, 2009; Pickering and Cantalejo, 2015); (iv) substantial parts of the source-to-sink system are preserved, from non-marine to deep-marine environments, including the basin margins; (v) the tectonic context of the basin is well understood, both at a regional (orogenic) scale and the development of the synsedimentary growth anticlines that bound the basin; (vi) the interfan "background" or fine-grained sediments have already revealed a record of Milankovitch cyclicity at precession, obliquity and short eccentricity scales (Heard *et al.*, 2008; Cantalejo and Pickering, 2014, 2015; Scotchman *et al.*, 2015), and (vii) there is a good understanding of Middle Eocene global climate (greenhouse period) and mean sea-level change that the Aínsa Basin stratigraphy can be placed within (*e.g.*, Miller *et al.*, 2005; Kominz *et al.*, 2008; Miller and Wright, 2017).

The Aínsa Basin is located in the footwall of the Montsec-Cotiella Thrust within the South Pyrenean Thrust System (Bentham and Burbank, 1996). The basin developed as a foreland basin during the Middle Eocene, due to flexural subsidence caused by the advancement of the Pyrenean deformation front (Puigdefábregas *et al.*, 1986, 1992; Dreyer *et al.*, 1999). As the thrust sheets propagated southward towards the foreland, two basin bounding anticlines developed, the Mediano and the Boltaña anticlines to the west and east, respectively (Mutti, 1983/84; Muñoz *et al.*, 1998, Fernández *et al.*, 2004). The continued development of these anticlines resulted in the Aínsa Basin becoming a thrust-top basin incorporated into the hangingwall of the Gavarnie-Sierras Exteriores thrust sheet (Muñoz *et al.*, 1998; Dreyer *et al.*, 1999; Fernández *et al.*, 2004; Pickering and Bayliss, 2009; Fernández *et al.*, 2012). Palaeomagnetic studies by Muñoz *et al.* (2013), supported by recent work (Cantalejo *et al.*, 2020) suggest regional clockwise vertical rotations of the Aínsa Oblique Zone of ~45–60° from early Lutetian to late Bartonian with the largest rotations (~40°) before ~42.5 Ma. We interpret that these large rotations were only possible once the Aínsa Basin was incorporated into the Gavarnie thrust sheet a thrust-top (piggyback) basin.

The infill of the Aínsa Basin consists of ~4 km of syntectonic slope, base-of-slope and proximal basin-floor deposits known as the Hecho Group (Mutti *et al.*, 1972; Remacha and Fernández, 2003; Fernández *et al.*, 2004; Pickering and Corregidor, 2005; Pickering and Bayliss, 2009). The basin succession comprises deep-marine sediment gravity-flow (SGF) deposits (definitions after Pickering and Hiscott, 2016) with thick intervals of thin-bedded,

laminated, siltstones and marlstones in units up to several hundred metres thick, interpreted as interfan and fan lateral-margin deposits interbedded with eight sand-rich, coarse-grained deep-marine systems (Pickering and Corregidor, 2005; Pickering and Bayliss 2009; Pickering and Cantalejo, 2015): from the oldest, they are named the Fosado, Los Molinos, Arro, Gerbe, Banastón, Aínsa, Morillo and Guaso systems. Each of these systems contains 2–6 sandy, channelised, submarine fans (Pickering and Corregidor, 2005).

The deep-marine sediments of the Aínsa Basin were sourced from an extensive fluvio-deltaic complex in the Tremp-Ager Basin (Montañana Group) (Mutti *et al.*, 1985; Marzo *et al.*, 1988) that transferred clastics into deep-marine environments via incised gullies and canyons (*e.g.*, the Charo Canyon) (Puigdefábregas *et al.*, 1992; Millington and Clark, 1995). Figure 1 is a summary stratigraphy of the Aínsa Basin.

There is a long-term 3–5 Myr tectonic driver in the Aínsa Basin that caused the development of angular unconformities that can be traced from the shelf to the deep-marine environments (Muñoz *et al.*, 1998; Arbués *et al.*, 1998; Remacha *et al.*, 2003; Pickering and Bayliss, 2009) (Figure 1). The stratigraphy of the Aínsa Basin can be divided broadly into two distinct successions: an older unit (Lower Hecho Group) that is structurally more deformed than the overlying unit that has an essentially layer-cake stratigraphy (Upper Hecho Group) (*e.g.*, Pickering and Corregidor, 2005).

Above the Atiart unconformity (Figure 1) that defined the onset of deep-marine deposits in the Aínsa Basin (Farrell *et al.*, 1987; Payros, *et al.*, 2009; Fernández, *et al.*, 2012), there is an ~2.5 Myr interval of essentially fine-grained (mudstone-dominated) sediments with isolated sandstones (or very thin packages of sandstones) before the first thick sandy Fosado fans. This stratigraphic interval and its timing is consistent with numerical models of hysteresis in an orogen where there is a time lag between tectonic uplift, denudation and river catchment reorganisation to deliver substantial coarse clastics via the fluvial and coastal systems (*e.g.*, Li *et al.*, 2018). For example, in the Zagros Mountains fold-and-thrust belt, Tucker and Singerland (1996) calculated a geomorphic response time up to a few million years. In the case of the Pyrenees, this hysteresis is specifically linked with the development of a deep-marine foreland basin on the foundered Tethyan (Mesozoic–Eocene) carbonate platform.

The submarine-fan model developed by Pickering and Corregidor (2005), modified by Pickering and Bayliss (2009), suggests that the typical facies distribution and stratigraphy observed in the Aínsa Basin can be explained by changes in relative base level (Figure 2). In

this model, an initial lowering of relative base level (*e.g.*, a sea-level fall or differential tectonic uplift/subsidence) could have triggered the accumulation of MTDs/MTCs. As the deep-water stratigraphy in the Aínsa Basin was fully marine (Pickering and Corregidor, 2005), the basin likely experienced any eustatic sea-level variation. As relative base level started to rise, sediment supply to the fan decreased and eventually resulted in fan abandonment. This model still appears broadly tenable irrespective of the driver/s on changing relative base level. There are however, some studies that have suggested that submarine fan initiation and MTD/MTC accumulation may result from high fluvial discharge not directly linked with sea-level falls (Nakajima and Itaki, 2007; Ducassou *et al.*, 2009; Covault and Graham, 2010; Covault *et al.*, 2010; Jorry *et al.*, 2011; Toucanne *et al.*, 2012). An increase in sediment supply from high fluvial discharge could potentially result in a similar facies architecture profile with the overall fining-upward trend of the submarine-fan being associated with a waning of the flooding events. However in this latter scenario, one might expect more MTDs/MTCs within the fan stratigraphy and not commonly linked with the base.

Methodology

We use orbital tuning to identify regular cyclostratigraphic periodicities in the Aínsa Basin sediments linked with astronomical frequencies. This method is used to refine the time scale of cyclostratigraphic analysis by aligning the geological records to the calculated orbital periodicities of Milankovitch cycles. Orbital tuning was first used by Hays *et al.* (1976) and since then, many researchers have used this method (*e.g.*, Imbrie *et al.*, 1984; Gale *et al.*, 1999; Bender, 2002; Weedon *et al.*, 2004; Westerhold *et al.*, 2013). Orbital tuning involves a two-step process. First, a band-pass filtering of the record is applied to the frequencies that are significant in the time-series and can be linked with orbital periodicities. These frequencies were then compared with the orbital history of eccentricity, obliquity and precession for that time interval.

This paper uses the cyclostratigraphic analysis of the gamma-ray logged sections presented in Cantalejo and Pickering (2015) to determine the main frequencies associated with eccentricity and obliquity cycles. The location of each of the gamma-ray logged sections can be seen in Figure 3. These sections were logged in continuous and undeformed fine-grained sediments interpreted mainly as interfan successions with minor channel levée-overbank

deposits. The Gerbe, Labuerda 2, Boltaña, Forcaz and Morillo sections have a good chronostratigraphic age control from recent biostratigraphic and magnetostratigraphic studies (Scotchman *et al.*, 2015; Cantalejo *et al.*, 2020).

Frequency-selective filtering

A band-pass filter was applied to the total gamma-ray records to show the amplitude of the signal and reflect the changing temporal importance of individual frequencies in the records. Only frequencies which consistently appeared in the spectra of the analysed data with confidence levels >90%, and that appear associated with eccentricity and obliquity orbital cycles using a combination of spectral techniques such as REDFIT, ASM and wavelet analysis, were applied for band-pass filtering (Cantalejo and Pickering, 2015). The program used for filtering is the Macintosh program Analyseries 2.0.3 (Paillard *et al.*, 1996). This program uses a band-pass Gaussian filter that modifies the original data by convolution with a Gaussian probability density function. This Gaussian function is centred at the specified frequency and the width of the function is determined by the filter bandwidth. The bandwidth used is the same as the one determined by spectral analysis using REDFIT. The filtered records for each of the analysed gamma-ray logged sections can be seen in Supplementary Material 1.

Orbital tuning

Orbital tuning was performed by comparing the total-gamma records presented in Cantalejo and Pickering (2015) filtered to the frequency associated with eccentricity (from REDFIT and ASM spectral analysis) to the historical eccentricity curves using the La2010a orbital solution of Laskar *et al.* (2011). The short eccentricity is the dominant cycle revealed by most of the time-series analysis. The control or anchor points used in the total-gamma filtered records are the depth points that constitute the top of each of the filtered cycles. These depth points were matched with the eccentricity maxima points in the La2010a orbital solution of Laskar *et al.* (2011). In those cases where the top of the cycles in the total-gamma filtered records show a poorly defined curve shape, then the anchor points used are the lowest point in the cycle and these were matched to eccentricity minima in the La2010a orbital solution of Laskar *et al.* (2011). The rest of the depth points in the total natural gamma time-series were matched to absolute time by using a simple linear interpolation between anchor points (Supplementary material 2).

The best evidence to show that orbital tuning was successful and that the time scale is accurate is reflected in a significant increase and sharpening of the orbital-frequency bands that were not tuned (Imbrie *et al.*, 1984, Muller and MacDonald, 2000). For example, successful orbital tuning may cause obliquity cycles to be strengthened and show an increase in spectral power when the records are tuned to eccentricity. However, authors have highlighted that coherency can also occur when the record has been aligned to the wrong set of orbital cycles or to the wrong part of the orbital history (Shackleton *et al.*, 1995; Weedon, 2005). In order to prevent this, a good chronostratigraphic record of the stratigraphy is required. Cantalejo *et al.* (2020) uses magnetostratigraphy in combination with calcareous nannofossils identification through the same gamma-ray logged sections (Cantalejo and Pickering, 2015). The three identified polarity reversals C21r–C21n, C21n–C20r and C20r–C20n enabled a more accurate orbital tuning of these sections to the eccentricity and obliquity curves of the Middle Eocene.

There are also risks associated to over-tuning the time-series records to match the target curve (Muller and MacDonald, 2000). Manipulating the data to match the target orbital curve may result in unphysical sediment accumulation rates (SARs). It is important, therefore, to check for each interval that SARs are consistent and do not show large spikes in the time-depth plot. SARs have been calculated for each of the tuned records and are presented in Supplementary material 3 and 4. The different attempts in tuning the gamma-ray records to the eccentricity curves are presented in Supplementary Material 5.

Results

The location of the gamma-ray logged sections can be seen in Figure 3. The gamma-ray logged sections tuned to the orbital solution of Laskar *et al.* (2011) are shown in Figure 4 (Gerbe section), Figure 5 (Labuerda 2 section), Figure 6 (Boltaña section), Figure 7 (Forcaz section), and Figure 8 (Morillo section). Figure 9 shows the spectral analysis using REDFIT of total-gamma records tuned to eccentricity. The stratigraphic position of each of the gamma-ray logged sections is summarised in Figure 10. For simplicity, we have included most of the analysis as supplementary material.

Orbital tuning of the Gerbe section

The stratigraphically oldest section that was logged is the ~200 m long Gerbe section, comprising the sediments between the Gerbe I to Banastón II fans. Orbital tuning of the Gerbe section used five anchor points. The best match between the total-gamma filtered records of the Gerbe section suggests that the base of this section can be dated at 47.36 Ma (Figure 4). This is in agreement with the age of the C21r–C21n polarity reversal found at the base of the section (~10 m stratigraphic height). The top of the Gerbe section, interpreted as the base of the Banastón II Fan, can be established at 46.93 Ma, giving a total duration for the Gerbe section of ~420-kyr. Figure 10 shows that tuning the records to eccentricity strengthens the power of the obliquity peak (~47-kyr). This peak can be matched with the obliquity O1 orbital period of 52-kyr which is then significant with confidence levels >99%. The peak at 32-kyr is also more prominent in the tuned data. This peak is likely to be associated with the obliquity O2 40-kyr orbital period. Tuning the records also strengthens the precession cycles P1 (~21-kyr) and P22 (~16-kyr) that were not significant in the untuned spectrum (<80% confidence levels). SARs for each of the intervals between the anchor points varied between 28.6–63.2 cm/kyr, with averaged values of ~47 cm/kyr.

Orbital tuning of the Labuerda section 2

The 350-m thick Labuerda section 2 is the longest undeformed gamma-ray logged section in the Aínsa Basin and is stratigraphically younger than the Gerbe section. Its base appears to be within the interfan sediments of the Banastón II Fan and the top is ~50 m below the base of the Aínsa I sandbody. Nine anchor points were used for tuning the records. The change in magnetic polarity from normal to reverse identified at ~185 m height correlates with the chron C21n–C20r magnetic reversal (Cantalejo *et al.*, 2020). The age of this reversal is estimated to have occurred at 45.72 Ma (Gradstein *et al.*, 2012). The best possible match, taking into consideration the position of this magnetic reversal in the records, establishes the beginning of Labuerda section 2 at 46.19 Ma. The top of the Labuerda section 2 is dated at 45.13 Ma, giving a total duration for the section of ~924-kyr.

Figure 10 shows that tuning the records to eccentricity strengthens the power of the obliquity peaks (52 and 42-kyr) which are now both present with >99% confidence levels. These peaks indicate that some variation in the duration of obliquity cycles is present in the records (*e.g.*, obliquity 52 and 40-kyr). Tuning the records also strengthens the precession cycles (P1 (26-

kyr) and possibly P2 (17-kyr). The precession peak P1 is now well above the >99% confidence level and the peak at 17-kyr is >95% confidence levels.

SARs calculated post-tuning of the Labuerda section 2 have sensible SARs that vary between 24.4 cm/kyr and 54.4 cm/kyr, with a mean values of ~35 cm/kyr. This SAR is very similar to the most representative SAR of the orbital periods for the Middle Eocene calculated by ASM analysis at 37 cm/kyr (Cantalejo and Pickering, 2015) and from palaeomagnetic studies at ~34.5 cm/kyr (Cantalejo *et al.*, 2020).

Orbital tuning of the Boltaña section

The Boltaña section is 167 m long and has its base in the interfan deposits of the Aínsa I Fan. The top of the section is close to the initiation of the Aínsa III Fan. A total of 6 anchor points were used for tuning the records. Magnetostratigraphic studies (Cantalejo *et al.*, 2020) show reverse polarity throughout the Boltaña section tied with chron C20r. The composite stratigraphy of the Aínsa Basin suggests that the top of the Labuerda section 2 and the base of the Boltaña section are very close stratigraphically and cannot be separated by more than ~50 m. Therefore, we estimate that the Boltaña section is located ~165–215 m above the C21n–C20r reversal at 45.72 Ma identified at ~185 m height in the Labuerda section 2. Comparison between the eccentricity curves of the La2010a orbital solution of Laskar *et al.* (2011) and the total-gamma, filtered records, shows a similar curve pattern (Figure 6). The well-developed eccentricity cycles of the first half of the Boltaña records and the loss of cycle definition in the top 60 m can be matched to the eccentricity curves of the La2010a orbital solution of Laskar *et al.* (2011) between ~45.3–44.7 Ma. Several attempts were undertaken to match the selected anchor points to the eccentricity maxima/minima points of the eccentricity curves of the orbital solution of Laskar *et al.* (2011) around this time interval (Figure 6). The best possible match between these two records suggests the Boltaña section was deposited between 45.29–44.56 Ma that is close to the initial estimation from stratigraphic study. The total duration of this section is 736-kyr.

The SARs of this section varied between 14.6–30.5 cm/kyr, with a mean value of ~24 cm/kyr. The averaged value is similar to the one calculated using ASM analysis that yielded an estimated averaged SAR of 26–30.5 cm/kyr (Cantalejo and Pickering, 2015).

Orbital tuning of the Forcaz section

The Forcaz section is ~185 m long and the sediments are younger than those of the Boltaña section. The top of the Boltaña section is located within the interfan deposits of the Aínsa II and Aínsa III sandy submarine fans. Thickness estimations from sedimentary logging suggest that the top of the Boltaña section is located ~50 m below the Aínsa III sandy fan (Cantalejo and Pickering, 2015). The Aínsa III sand fan in the Forcaz section is represented by a 15 m heterolithic package located at 30–45 m height. Therefore, it is reasonable to assume that the beginning of the Forcaz section coincides approximately with the end of the Boltaña section. The base of the Forcaz section should, therefore, have accumulated close to ~44.56 Ma. Eight anchor points were used for tuning the records. Magnetostratigraphic studies show reverse polarity throughout the Forcaz section (Cantalejo *et al.*, 2020), interpreted to be chron C20r (45.72–43.43 Ma, Gradstein *et al.*, 2012). The best curve match between the anchor points and the eccentricity maxima points around this time interval and the best response in the time-series analysis are shown in Figure 7. The interval between 60–90 m height has undergone more manipulation to match the total-gamma filtered records to the eccentricity cycles of the orbital solution, whilst the rest of the data remained mostly unchanged. Although, there is no significant strengthening of the spectral peaks after tuning, the three main orbital parameters (eccentricity, obliquity and precession) are present with confidence levels >99% (Figure 10). The Forcaz section most likely accumulated between 44.63–44.02 Ma with a total duration of ~615-kyr.

Calculating the SAR for each stratigraphic interval in the Forcaz section gives 16.3 cm/kyr and 50.5 cm/kyr, with a mean value of ~29.4 cm/kyr. This averaged SAR value is close to the SAR calculated using ASM analysis of 33 cm/kyr (Cantalejo and Pickering, 2015) and similar to the 28.5 cm/kyr SAR calculated in sediment cores of similar age (Well A6 core in Cantalejo and Pickering, 2014). The Forcaz section (~185 m) and the A6 core (150 m of undeformed sediments) mostly fully overlap, *i.e.*, the undeformed A6 core has an overlap of ~100–120 m with the Forcaz section. Cantalejo and Pickering (2014) studied the geochemistry and sedimentology of the Aínsa Well A6), and based on core-to-outcrop correlations, we estimate that the Forcaz starts ~30 m earlier and the A6 core ends in an MTC close to the initiation of the Morillo I sandy fan.

Orbital tuning of the Morillo section

As the Morillo section is the shortest of all the gamma-ray logged sections at 123 m in stratigraphic thickness (Cantalejo and Pickering, 2015), the total gamma records therefore have been tuned to the obliquity cycle, which has reduced the confidence of our estimations. Ten anchor points have been used for tuning the records.

Age estimations using biostratigraphic studies suggest the Morillo System was deposited between 43.2–44.24 Ma (late Lutetian); during nannofossil zone NP15–NP16 and shallow benthic foraminifera zone SBZ14–SBZ15 (Scotchman *et al.*, 2015). These estimated ages are in agreement with studies from Mochales *et al.* (2012a) who estimated the end of the Morillo System at 43.2 Ma. 43.9–44.9 Ma (middle Lutetian), during nannofossil zone NP15 and shallow benthic foraminifera zone SBZ13–SBZ14 (Scotchman *et al.*, 2015).

Magnetostratigraphic studies show reverse polarity throughout the Morillo section, likely to be chron C20r (45.72–43.43 Ma) (Gradstein *et al.*, 2012) with a polarity reversal to normal polarity at the base of Morillo III Fan (C20r–C20n boundary) (Cantalejo *et al.*, 2020).

Thickness estimations from sedimentary logging suggest that the top of the Morillo section is located at the base of the Morillo III Fan by a thick MTC. It is reasonable to assume that the top of the Morillo section is very close to the C20r/C20n reversal at 43.43 Ma. The best curve match and the best response in the time-series analysis are shown in Figure 8. There is a significant strengthening of the spectral peaks after tuning, with obliquity and precession present at confidence levels >99% (Figure 10). Tuning the total-gamma data to other obliquity cycles reduces the confidence levels of the precession cycles significantly (Supplementary Material 5). The Morillo section, therefore, was more likely deposited between 43.64–43.42 Ma with a total duration of ~220-kyr. The SAR for each stratigraphic interval in the Morillo section gives a variation between 14.5 and 22.5 cm/kyr, with a mean value of ~19 cm/kyr.

Sub-Milankovitch climate signals in the Aínsa Basin (LLTM)

In deep-marine basins, hyperthermal events are recorded in sediments as a clay-rich layer indicating dissolution of carbonate (Lourens *et al.*, 2005; Zachos *et al.*, 2005; Leon-Rodriguez and Dickens, 2010). Also, in studies of core data from the North Sea hyperthermals have been recognised with high total gamma-ray readings in core logs (*e.g.*, Kender *et al.*, 2012; Kemp *et al.*, 2016). The Late Lutetian Thermal Maximum (LLTM) has been defined as a short-lived (~30-kyr) transient global warming event that occurred at ~41.5

Ma in the late Lutetian within magnetochron C19r, and was characterised by an $\sim 2^{\circ}\text{C}$ warming of the deep ocean in the southern South Atlantic (Westerholet *et al.*, 2018). These authors described the event in three cores from the South Atlantic (ODP sites 1260, 1263 and 702), in which the LLTM occurs as a dark-coloured clay-rich band and XRF scanning of these cores show a distinctive peak in Fe intensities, decrease in carbonate content and negative CIE (carbon isotope excursion) of 0.86. The clay-rich layer with lowered carbonate content with respect to the average normal concentration was estimated to last ~ 15 -kyr.

In the Aínsa Basin, the candidate LLTM is a prominent (with a few subsidiary) 3 metres thick, basin-wide black mudstones/claystones band (Figure 11), unique to the basin, and mappable above the youngest submarine fan in the Guaso System. Our new age model dates this band at ~ 41.5 Ma within Chron 19 (Cantalejo, *et al.*, 2020). Figure 11 is a 40 m-thick sedimentary section that we logged through this interval with a hand-held spectral gamma-ray tool. Sediments in this interval are characterised by a fine-grained succession of marlstones and siltstones with rare thin-bedded cm-scale fine-grained sandstone turbidites. Paler-coloured bands probably represent carbonate-rich cemented bands. The thin nummulite-rich layers have been interpreted as storm-triggered turbidites (Cantalejo and Pickering, 2014). The dark-grey ~ 3 m layer is located towards the upper part of the log (Figure 12). High-resolution gamma-ray logging shows that the dark bands are characterised by an increase in the total gamma and K readings, which we believe are associated to an increase in clay content. There is also a tendency for greater Th content across the section.

Time-series analysis of the mudrocks in the Aínsa Basin have revealed a Milankovitch forcing on the finer-grained, interfan, sediments and suggest sediment accumulation rates (SARs) of ~ 30 – 35 cm/kyr (Cantalejo and Pickering, 2014, 2015), consistent with the interval containing the dark mudstones/claystones as the LLTM. As the LLTM is an ~ 30 -kyr global transient hyperthermal event, dated at 41.52 Ma (*cf.* Westerhold *et al.*, 2018), this would suggest that its duration as a stratigraphic thickness should be ~ 10 m, consistent with the LLTM at outcrop encapsulating both dark bands, at ~ 23 m and ~ 29 – 32 m in the log shown in Figure 12.

Discussion

In this section, we discuss the main drivers that may have been responsible to the delivery of coarse sediment supply to the Aínsa Basin.

Eustatic control on the deposition of the Aínsa Basin sandy fans

Figure 13 shows the orbitally-tuned stratigraphy of the Aínsa Basin and the eccentricity curves of the La2010a orbital solution of Laskar *et al.* (2011). Periods of eccentricity minima are shown. The figure also presents a high-resolution eustatic sea-level curve for the Middle Eocene. This sea-level curve shows a general decrease in sea level of 10s m (with higher frequency sea-level variations) from the Arro System towards the Guaso System. Pickering and Bayliss (2009) suggested that the deposition of the twenty-five sandy submarine fans in the Aínsa Basin could have been controlled by glacio-eustatic changes linked to the ~400-kyr Milankovitch eccentricity frequency. Although the presence of glaciation during the Middle Eocene remains controversial, there is growing evidence that supports the presence of at least ephemeral ice-sheets that resulted in moderate (20–40 m) high-frequency global sea-level changes during this time period (Haq *et al.*, 1987; Miller *et al.*, 2005; Kominz *et al.*, 2008; Tripathi and Darby, 2018). Many studies have linked ice-sheet initiation and expansion to periods of reduced insolation during the 400-kyr eccentricity minima (Zachos *et al.*, 2001b; Pälike *et al.*, 2006a, b; Liebrand *et al.*, 2011). The storing of water as groundwater (and lakes) on the continents, also known as aquifer-eustasy, although still not well recognised in the stratigraphy record, is an alternative mechanism for similar scale sea-level changes paced by long-term eccentricity cycles during warm greenhouse where ice-sheets were absent (Sames *et al.*, 2016, 2020).

Conventional Milankovitch theory asserts that orbitally-induced changes in high-latitude summer insolation control the waxing and waning of ice sheets, and that precession should dominate the ice-volume response as it most strongly modulates summer insolation. Ruddiman (2006) argued that the dominant 100-kyr response of ice sheets appears to lie mainly in internal feedbacks (CO₂ and ice albedo) that drive the gradual build-up of large ice sheets and their subsequent rapid destruction. Ice melting during terminations is initiated by uniquely coincident forcing from insolation and greenhouse gases at the periods of tilt and precession. However, in a study by Tabor *et al.* (2014), using an Earth system model coupled with a dynamic ice sheet to separate the climate responses to idealised transient orbits of obliquity and precession that maximise insolation changes for the early Pleistocene (2.588–0.781 Ma), they found that ice-volume proxy records vary almost exclusively at the frequency of the obliquity cycle. Our field-based study recognises a dominant eccentricity and obliquity 41-kyr signal (Figure 10).

Our study shows that over ~8 Myr in the Middle Eocene, the long eccentricity (400-kyr) Milankovitch cyclicity is likely archived in the accumulation of ~72% of the sandy submarine fans in the Aínsa Basin stratigraphy. We only include those sandy fans that contain good radiometric control from the Gerbe to the Guaso systems and discount those from the Lower Hecho Group characterised by complex structural deformation with no tuned sections available. Figure 13 suggests that many of the submarine fans were initiated during periods of 400-kyr eccentricity minima, which tend to coincide with eustatic sea-level lows. However, there is a much more complicated climatic relationship between any possible eustatic sea-level variations and the timing of deposition for each of the Aínsa deep-marine sandy submarine fans. Our study suggests that submarine-fan development linked with eccentricity cycles with periodicities of ~95-kyr, 123-kyr and 400-kyr are likely to have been more regular and periodic than the timing of fan initiation estimated from this study and, therefore, we conclude that if this mechanism was the principal driver for the deposition of the twenty-five submarine fans of the Aínsa Basin, then such climate signals were not surprisingly complex (*cf.* Ruddiman, 2006).

Other study has revealed the importance of both the short and long eccentricity in deep-marine sediments, *e.g.*, the Oligocene (Wade and Pälike, 2004) and Middle Miocene global ice volume and ocean carbon reservoir changes as recorded in deep-sea records, respectively (Shevenell *et al.*, 2004; Holbourn *et al.*, 2005; Westerhold *et al.*, 2018). Some modelling results have also highlighted the dominant long eccentricity (400-kyr) forcing on the Middle Miocene climate change (DeConto and Pollard, 2003; Ma *et al.*, 2011; Tian *et al.*, 2013). Results from climate models for low-latitude late Palaeozoic successions have suggested that both high-latitude ice-sheet accumulation and ablation, and low-latitude climate change were paced by the eccentricity. Periods of high eccentricity amplified precession-driven changes in insolation and promoted high-latitude ice sheet volume fluctuations as well as increased low-latitude precipitation variability. When eccentricity was low, the amplification of precession-driven insolation fluctuations was reduced, which promoted high-latitude continental ice sheet stability and less variable low-latitude precipitation (Horton *et al.*, 2012).

A strong climatic 400-kyr signal is identified in the early Eocene (Smith *et al.*, 2014), and the Palaeocene (greenhouse conditions) deep-marine Zumaya section in northern Spain (Dinarés-Turell *et al.* (2003). The Zumaya section comprises rhythmic alternations of pink-reddish-grey hemipelagic limestones and marlstones, plus some intercalations of thin-bedded carbonate turbidites. Also, in a sedimentological and geochemical analysis of

palaeogeographically and temporally related early–middle Eocene hemipelagic successions in the Basque–Cantabrian Basin, comprising hemipelagic limestone–marl alternations, Martinez-Braceras *et al.* (2017) recognise astronomically-regulated precession cycles of 21-kyr modulated by orbital eccentricity cycles of 100-kyr. Thus, in sediments of the same age as the siliciclastics in the Aínsa Basin, and in linked marine basins, a strong climatic signal has been identified.

Castelltort *et al.* (2017) used a high-resolution carbon isotope stratigraphy in an attempt to provide an independent record of global sea-level changes for the Arro, Gerbe and lower Banastón systems (first investigated in a pilot study for the Aínsa Basin by Das Gupta, 2008, Figure 7.4). Castelltort *et al.* (2017) proposed that the bulk $\delta^{13}\text{C}_{\text{carb}}$ signal accurately correlated with the coeval eustatic curve from the New Jersey (USA) passive margin based on the backstripped curves of Miller *et al.* (2005), and that the sandy fans accumulated during eustatic lowstands and fine-grained marly interfan sediments correlate with rising and highstand sea levels (as proposed by Pickering and Bayliss, 2009, Figure 6). However, they also asserted that the sandy Arro Fan accumulated during a sea-level highstand, that could be associated with changes in fluvial discharge. Our new palaeomagnetic study and age model for the Aínsa Basin (Cantalejo *et al.*, 2020) using a higher-resolution eustatic sea-level curve (Figure 13), suggests that the Arro-I and Arro-II sandy fans coincide with high-frequency eustatic falls (and eccentricity minima), whereas with a lower-resolution (smoothed) eustatic curve, as used by Castelltort *et al.* (2017) to argue for a highstand for the Arro System, the opposite conclusion can be reached. This apparent contradiction, therefore, highlights the inherent problems in applying low-resolution eustatic curves to investigate climatic/eustatic *versus* tectonic controls on sediment flux. Higher resolution eustatic curves can lead to a contrary interpretation.

In the Jaca Basin, Huyghe *et al.* (2012) described cyclic carbonates and explained them as due to high-amplitude, high-frequency (<100-kyr) glacio-eustatic sea-level changes. Also, Gómez-Paccard *et al.* (2011) documented composite sequences in the Montserrat alluvial fan/fan-delta complex of the Ebro Basin, which they interpreted as 400-kyr long eccentricity cycles, possibly controlled by sea-level fluctuations. Outcrop studies in other Paleogene deep-marine systems throughout the Spanish Pyrenees have already been shown to preserve an archive of Milankovitch cyclicity with the long eccentricity as an important control on depositional processes (Gómez-Paccard *et al.*, 2011; Batenburg *et al.*, 2012).

Fluviatile discharge control on the deposition of the Aínsa Basin

An increase of coarse-grained supply to the deep-marine environment during a period of eccentricity maxima could have been linked to intense rainfall and flash floods. This may be the case of the Gerbe II Fan (Figure 13), but this might have been linked with tectonic activity and basin reconfiguration as the Aínsa Basin was transformed into a thrust-top basin (see below section on tectonic controls). However, we note that whilst the Gerbe-II, Banastón-V and Morillo-I fans appear to be at eccentricity maxima, all three accumulated during longer-term eustatic falling sea level.

The relatively small width (~20 km) of the Aínsa Basin, the presence of a narrow shelf typical of tectonically active margins (Milliman and Syvitski, 1992), and the narrowly focussed principal sediment source/s at the eastern end of the Aínsa Basin were associated with submarine fans being fed directly from terrestrial and coastal areas with cycles of fan initiation and abandonment reflecting orbitally-induced climate changes (Weltje and de Boer, 1993).

Milliman and Syvitski (1992) suggest that rivers in tectonically active margins are more susceptible to periodic floods that can discharge large amounts of sediment into deep water, even during highstands. Basin geomorphological factors can facilitate the transport of sediment from fluvial and deltaic to deep-marine environments, with small drainage basins and the presence of narrow shelves being most favourable to such processes (Milliman and Syvitski, 1992; Couvaut and Graham, 2010). In the Tremp Basin, high-frequency climate change has been identified within the fluvio-deltaic sediments of the Montañana Group (*e.g.*, Weltje *et al.*, 1996; Nijman, 1998).

In the Western Pyrenees, Payros and Martinez-Braceras (2014), in a study of the Gorrondatxe section (Global Stratotype Section and Point for the base of the Lutetian Stage in the western Pyrenees), showed that the characteristics of lower–middle Eocene fan-fringe/basin-plain deep-marine siliciclastic and pelagic deposits varied in line with orbitally-forced fluctuations in seasonal rainfall, runoff and terrigenous input. Reduced SGF activity during the formation of pelagic limy precession hemicouplets suggested subdued seasonality and low terrigenous input. Conversely, sandy SGFs were more frequent, had greater energy and were more voluminous during the formation of pelagic marly hemicouplets, suggesting precession hemicycles with strong seasonality and heavy summer rainfall. They found that these differences at precession timescales were enhanced at maximum eccentricity because sandy SGF activity was most intense during the boreal summer at perihelion (*i.e.*, maximum seasonality), but declined at aphelion. At minimum eccentricity, with relatively weak seasonality throughout one (or more) precession cycle (>21-kyr), sandy SGF activity remained relatively low. These patterns in the Gorrondatxe fan-fringe/basin-plain succession suggest that the orbitally-forced environmental changes must also have affected the inner and middle parts of the submarine fan. The astronomical influence on terrigenous sediment input also determined the changing characteristics of the pelagic sedimentation. The terrigenous contribution to pelagic sedimentation fluctuated by a factor of five during opposite precession times at maximum eccentricity, whereas there was almost no fluctuation at minimum eccentricity, a situation that seems the converse for most Aínsa Basin sandy fans.

Also, Kodama *et al.* (2010) deduced orbitally-induced changes in magnetite content in Eocene marine marlstones of the Pamplona-Arguis Formation, Spanish Pyrenees, which they interpreted as caused by periodic variations in precipitation, fluvial discharge and terrigenous supply during the rainy season.

Although this mechanism may explain some of the sandy fans, our results suggest that is not dominant in the deep-marine sediments of the Aínsa Basin.

Tectonic control on the deposition of the Aínsa Basin sandy fans

It can be argued that the aperiodic timing for the deposition of the twenty-five principal sandy fans in the Aínsa Basin could partially be explained by tectonic processes. The growth of the synsedimentary Mediano Anticline could have increased the gradient of the depositional profile, leading to a local relative sea-level fall, probably of low to moderate amplitude (*cf.* Mutti *et al.*, 2003). The intermittent growth of the Mediano Anticline at time intervals in the order of <1–1.5 Myr has been linked to the episodic movement of the Cotiella-Montsec (Gavarnie) thrust sheet and as a potential driver identified in the formation of the so-called “tectonostratigraphic units” (Holl and Anastasio, 1993; Muñoz *et al.*, 1998; Arbués *et al.*, 1998; Remacha *et al.*, 2003; Pickering and Corregidor, 2005). Such postulated episodes of anticline growth would have resulted in relative lowering of the base level that may have triggered MTD/MTC deposition and coarse clastics being stripped from the coastal and narrow shelf areas to accumulate as sandy submarine fan deposits in the Aínsa Basin.

Tectonic processes likely exerted a significant control on sediment delivery towards the end of the Lower Hecho Group when the Gerbe II Fan appears to have accumulated closer to a 400-kyr long-eccentricity maxima (Figure 13). The Upper Hecho Group (Banastón, Aínsa, Morillo and Guaso systems) shows an essentially gently folded layer-cake stratigraphy in the gently plunging open Buil Syncline. In contrast, the Lower Hecho Group (Fosado, Los Molinos, Arro and Gerbe systems) underwent substantial shortening to be sheared, folded and thrust so that the western limb became locally overturned. We believe that this tectonic activity was directly linked with the incorporation of the Aínsa Basin into the Gavarnie thrust sheet as a thrust-top basin, synchronous with the growth of the Mediano Anticline. Such intense tectonism could have been associated with the stripping of sand from shallow-marine and coastal environments and the accumulation of sand in the deep basin.

Clockwise vertical axis rotations (CVAR) of 60–45° occurred for the Aínsa Basin from early Lutetian to late Bartonian when the folds and thrusts of the Aínsa Oblique Zone developed (Muñoz *et al.* 2013). In the early Lutetian (~48 Ma), the Boltaña and Mediano anticlines were undeveloped as basin-bounding structures (Muñoz *et al.*, 2013, Figure 17). Palaeomagnetic

data for the clockwise vertical-axis rotations of the Mediano and Boltaña anticlines show that after 47.5 Ma (coinciding with the fine-grained interfan sediments between the Gerbe I and Gerbe II sandy fans) they follow a decreasing exponential function with most of the rotations between 47.5–42.5 Ma (Muñoz *et al.* 2013, Figure 14), i.e., between the Gerbe I and Guaso I systems (Upper Hecho Group). As argued above, we suggest that the beginning of this period of large-scale CVAR marks the time when the Aínsa Basin was converted from a foreland basin *sensu stricto* to a thrust-top (piggyback) basin as it was an integral part of the Gavarnie thrust sheet lubricated by the underlying weak evaporite horizons at the bottom of the detached Mesozoic and Paleogene successions (Muñoz *et al.*, 2013). The large-scale CVAR would have been kinematically easier after the Aínsa Basin became a thrust-top basin. A second rotation event, Late Eocene-Oligocene in age, added a further 10° of CVAR (Muñoz *et al.*, 2013).

Several studies suggest that fault displacements accumulate at relatively uniform rates over time-periods between 20-kyr and 300-kyr whilst very high-frequency fault displacements (<20-kyr) are highly variable (Nicol *et al.*, 1997, 2005; Mouslopoulou *et al.*, 2009). Clevis *et al.* (2003) used numerical modelling to study the effects of regular pulsating tectonic activity on basin drainage morphology. They simulated tectonic pulses of 200-kyr duration followed by periods of tectonic quiescence of the same time duration. Their results showed a pattern of periodic stratigraphic alternation of prograding and retrograding alluvial-fan gravels. Periods of tectonic activity were associated with alluvial fan and coastline retreats and tectonically-quiescent periods were associated with the cessation of flexural subsidence, progradation of the alluvial fans and increased delivery of gravels to the basin. Clevis *et al.* (2003) suggested that coastal retreat during periods of tectonic uplift occurred because delta catchment yields were insufficient to fill the accommodation created by flexural subsidence in response to tectonic loading.

The episodic (but likely aperiodic) tectonic uplift recognised in the Mediano Anticline (Holl and Anastasio, 1993) could have resulted in intermittent delivery of coarse-grained sediment to the Aínsa Basin. The lag-time between tectonic uplift and delivery of coarse-grained material that was computer modelled by Clevis *et al.* (2003) suggested an order of tens to hundreds of thousands of years between the deposition of the sandy fans postulated to have occurred between periods of significant uplift (growth) of the Mediano Anticline. The numerical model of Clevis *et al.* (2003) also suggested that greater fault displacement rates resulted in higher average SARs during decreased thrust activity. These tectonic processes

could explain the high SARs observed during the deposition of the Arro and the Gerbe systems after the significant period of growth of the Mediano Anticline during chron C22r (Figure 14). It was at that time that the Lower Hecho Group stratigraphy was intensely deformed to such an extent that the sandy fans and associated sediments were sheared and folded into large-scale recumbent folds prior to the accumulation of an essentially layer-cake stratigraphy observed for the Upper Hecho Group.

Various researchers have argued for both a dominant tectonic control and/or a mixed tectonic-climatic forcing to drive sediment supply in the Middle Eocene sediments of the Pyrenees. For example, Peper and de Boer (1995) applied a numerical model to the Trespaderne Basin to explain cyclical changes in sediment supply for coarse clastic flux in the deltaic parasequences as due to both climatic forcing and regular tectonic pulses. However, as has been true for many similar studies, the lack of a robust chronostratigraphic framework calls into question such interpretations.

In the Aínsa Basin, one might reasonably argue that both climate and tectonics influenced the accumulation of the sandy submarine fans. In the numerical modelling discussed above, Clevis *et al.* (2003) added small-scale (~20 m) sea-level variations controlled by 100-kyr Milankovitch eccentricity. The combination of tectonic and climatic variables resulted in a complex stratigraphic pattern. Although major progradation events associated with the tectonic pulses could still be recognised, the tectonic signal was clearly obscured by the high-frequency climatic sea-level fluctuations. The results of this numerical model are comparable temporally with the stratigraphic framework of the Aínsa Basin, although it is more likely that the tectonic growth pulses of the Mediano Anticline were more irregular than the input pulses in this numerical model. The initiation of the Aínsa fan systems could have resulted following major pulses of tectonic growth whilst some individual submarine fans, MTDs and smaller heterolithic packages may have been associated with small-scaled climatic variations controlled by orbital cycles. Cyclic climatic processes responsible for the sediment packaging of the fine-grained successions are likely to have been locally obscured by aperiodic tectonic processes, such as the growth of the Mediano, Boltaña and Añisclo anticlines.

There is evidence of other growth anticlines within the Aínsa Basin that were active during the deposition of the sandy fans and they may have influenced stacking patterns and avulsion of the submarine fans. For example, Bayliss and Pickering (2015) discuss the growth of the

Añisclo Anticline and its role in the deposition of the Banastón System fans. This growth could be considered as a tectonic control and a driver of autocyclic processes.

Autocyclic control on the deposition of the Aínsa Basin sandy fans

Autocyclic processes may produce repeating depositional cycles and although some of these processes are intrinsic to the depositional system, they are commonly aperiodic (Cecil, 2013). The cyclic but irregular nature of autogenic processes could be a possible mechanism for the irregular timing of the coarse-grained deposition of the Aínsa Basin. However, Pickering and Bayliss (2009) argue against an autocyclic control for the deposition of the Aínsa Basin sandy fans as the deposition and architecture of these sandy fans cannot be explained by lateral switching and compensational stacking processes. The two main arguments cited against autocyclic processes are: (i) the westward shift of the sandy fans towards the foreland and away from the deformation front, explained by the differential growth of basin-bounding anticlines, and (ii) the switching on and off of coarse-grained sediment with thick intervals of interfan fine-grained deposits between sandy fans, implying an external forcing on the influx of coarse-grained sediment to the basin. Autocyclic processes, however, may still have played a role in controlling the distribution of sandy sediment at shorter temporal and spatial scales. Pickering and Corregidor (2005) recognised within the internal architecture of each submarine fan several cycles of erosional channel incision, sediment bypass and channel infill (backfill) that they attributed to possible autocyclic processes.

Conclusions

The first-order, long-term, control on the accommodation for the coarse-grained clastic sediments to the Aínsa Basin was both extrabasinal and intrabasinal tectonics (cf. Pickering and Bayliss, 2009). The punctuated growth of the Mediano Anticline may have caused episodic reduction of accommodation on the shelf, leading to forced regressions and a concomitant increased flux of relatively coarse-grained sediments into the deep basin linked to sandy submarine fan development. However, orbital tuning of gamma-ray logged interfan and levée-overbank sections to the eccentricity curves, permitting the conversion of a depth-stratigraphy to an age-stratigraphy, suggests that like the finer-grained sediments the accumulation of at least several of the sandy fans likely had a strong climatic driver

expressed by the 400-kyr eccentricity cycles, with fan growth tending to occur linked to eccentricity minima.

Our magnetostratigraphically-calibrated chronostratigraphy for the sediments of the Upper Hecho Group (Gerbe, Banastón, Aínsa and the lower part of the Morillo System) allows the estimation of the age of initiation of the deep-marine systems and of individual sandy fans. The Gerbe System is estimated to have been initiated at 47.73 Ma, the Banastón System at 46.97 Ma and the Aínsa System at 45.16 Ma. Note that with tuning of our stratigraphic intervals using time-series analysis (this paper), there is a discrepancy between these ages and those presented in Cantalejo *et al.* (2020). These differences are too small to resolve biostratigraphically as they represent up to several hundred thousand years.

The interfan and levée-overbank deposits in the Aínsa Basin have already been shown to contain a strong Milankovitch cyclicity. Orbital parameters most likely paced the regular delivery of the fine-grained sediment mainly by river-derived (hyperpycnal) turbidity currents. Our time-series analysis of fine-grained stratigraphic sections throughout the Aínsa Basin suggests that, irrespective of if they represent interfan or channel-levée successions, they contain a similar archive of Milankovitch forcing. This conclusion emphasises the incomplete record of the processes forcing coarse sediment flux into and through the channels. Most of the SGFs travelling through the submarine channels will have left no clear depositional record of their transit, other than in the levée-overbank deposits. The pacing of the coarse-grained submarine fans, however, cannot be entirely explained by climatic forcing.

Our results suggest that the apparently variable recurrence time and duration of each sandy submarine fan was complex and cannot support the simple hypothesis that the 400-kyr eccentricity cycles alone paced the delivery of all the coarse-grained material to the basin. The majority of sandy submarine fans, however, coincide with periods of long-eccentricity (400-kyr) minima, suggesting that many of these sandy fans may have been modulated by climate changes influenced by Milankovitch parameters. The most likely explanation is that a eustatic driver was responsible for the accumulation of most of the sandy submarine fans. At certain times in the evolution of the Aínsa Basin, tectonic processes appear to have exerted a more important control on sediment delivery towards the end of the Lower Hecho Group (Gerbe System). During this period, the Aínsa Basin was undergoing major structural reorganisation, probably becoming a thrust-top (piggyback) basin in the Gavarnie thrust sheet. Finally, autocyclic processes may have caused internal reorganisation of sediment

within fan architecture (at the scale of individual channels and lobes) with many cycles of channel incision, sediment bypass and infill identified in each submarine fan succession: these processes alone cannot explain the sedimentary and stratigraphic architecture of the sandy fans in the basin.

Together with recognising a strong climate signal at a range of Milankovitch scales for the fine-grained deep-marine clastic sediments in the Aínsa Basin, we also identify sub-Milankovitch climate signals as in the ~41.5 Ma Late Lutetian Thermal Maximum (LLTM).

Our study is the first detailed study of a deep-marine basin where both the age model and data come from the same sediments, and that integrates this data with the entire stratigraphy over ~8 Myr. This has led to a greater level of confidence in our results and conclusions. We have shown that climate change and eustasy were likely the principal drivers on the accumulation of many of the sandy submarine fans at a time when many researchers invoke a greenhouse world. However, we also show that the causal processes were complex and likely also involved some tectonic control, and probably hysteresis effects for the sediment flux. An important outcome from our results is that there remains a need for even higher-resolution climatic and eustatic data if we are to effectively deconvolve the causal processes on clastic sediment delivery to deep-marine basins. There remains a need to understand not only changing relative sea level, but also the amplitude-frequency and duration of such changes linked with the availability of coarse sediment for redeposition in sandy submarine fans.

References

- Anka, A. and Séranne, M. 2004. Reconnaissance study of the ancient Zaire (Congo) deep-sea fan (ZaiAngo Project). *Marine Geology*, **209**, 223–244.
- Arbués, P., Muñoz, J.A., Poblet, J., Puigdefàbregas, C. and McClay, K. 1998. Significance of submarine truncation surfaces in the sedimentary infill of the Aínsa basin (Eocene of south-central Pyrenees, Spain). *15th International Sedimentological Congress, Alicante, Spain*, Publicaciones de la Universidad de Alicante, 145–146.
- Armitage, D.A., Piper, D.J.W., McGee, D.T. and Morris, W.R. 2010. Turbidite deposition on the glacially influenced, canyon-dominated Southwest Grand Banks Slope, Canada. *Sedimentology*, **57**, 1387–1408.

- Babonneau, N., Savoye, B., Cremer, M. and Klein, B. 2002. Morphology and architecture of the present canyon and channel system of the Zaire deep-sea fan. *Marine and Petroleum Geology*, **17**, 445–467.
- Backert, N., Ford, M. and Malartre, M. 2010. Architecture and sedimentology of the Kerinitis Gilbert-type fan delta, Corinth Rift, Greece. *Sedimentology*, **57**, 543–586.
- Barker, P.F. and Camerlenghi, A. 2002. Glacial history of the Antarctic Peninsula from Pacific margin sediments. *In*: Barker, P.F., Camerlenghi, A., Acton, G.D. and Ramsay, A.T.S. (eds), *Proceedings of the Ocean Drilling Program, Scientific Results*, **178**, 1–40. College Station, Texas, USA: Ocean Drilling Program.
- Barnolas, A. and Gil-Peña, I. 2001. Ejemplos de relleno sedimentario multiepisódico en una cuenca de antepaís fragmentada: La Cuenca Surpirenaica, *Boletín Geológico y Minero*, **112** (3), 17–38.
- Batenburg, S.J., Sprovieri, M., Gale, A.S., Hilgen, F.J., Hüsing, S., Laskar, J., Liebrand, D., Lirer, F., Orue-Etxebarria, X., Pelosi, N. and Smit, J. 2012. Cyclostratigraphy and astronomical tuning of the Late Maastrichtian at Zumaia (Basque country, Northern Spain). *Earth and Planetary Science Letters*, **359–360**, 264–278.
- Beekman, F., Bull, J.M., Cloetingh, S. and Scrutton, R.A. 1995. Crustal fault reactivation as initiator of lithospheric folding in the Central Indian Ocean. *In*: Nieuwland, D. (eds), *Modern examples in structural interpretation, validation and modelling*, 251–263. Geological Society London, Special Publication, **99**.
- Bender, M.L. 2002. Orbital tuning chronology for the Vostok climate record supported by trapped gas composition. *Earth and Planetary Science Letters*, **204**, 275–289.
- Bentham, P. and Burbank, D.W. 1996. Chronology of Eocene foreland basin evolution along the western oblique margin of the South-Central Pyrenees. *In*: Friend, P.F. and Dabrio, C.J. (eds), *Tertiary basins of Spain: the stratigraphic record of crustal kinematics*, 144–152. World and Regional Geology, **6**. Cambridge University Press. ISBN: 0 521 46171 5
- Bentham, P. 1992. *The tectono-stratigraphic development of the western oblique ramp of the South-Central Pyrenean thrust system, Northern Spain*. PhD Thesis, University of Southern California. 253 pp.

- Blum, M.D. and Tornqvist, T.E. 2000. Fluvial responses to climate and sea-level change: a review and look forward. *Sedimentology*, **47**, 2–48.
- Bouma, A.H., Coleman, J.M., Stelling, C.E. and Kohl, B. 1989. Influence of relative sea level changes on the construction of the Mississippi fan. *Geo-marine Letters*, **9**, 161–170.
- Bourget, J., Zaragosi, S., Rodriguez, M., Fournier, M., Garlan, T. and Chamot-Rooke, N. 2013. Late Quaternary megaturbidites of the Indus Fan: Origin and stratigraphic significance. *Marine Geology*, **336**, 10–23.
- Burgess, P.M. and Hovius, N. 1998. Rates of delta progradation during highstands: Consequences for timing of deposition in deep-marine systems. *Geological Society of London*, **15**, 217–222.
- Cantalejo, B. and Pickering, K.T. 2014. Climate forcing of fine-grained deep-marine systems in an active tectonic setting: Middle Eocene, Aínsa Basin, Spanish Pyrenees. *Palaeogeography, Palaeoclimatology, Palaeoecology*, **410**, 351–371.
- Cantalejo, B. and Pickering, K.T. 2015. Orbital forcing as principal driver for fine-grained deep-marine siliciclastic sediments, Middle-Eocene Aínsa Basin, Spanish Pyrenees. *Palaeogeography, Palaeoclimatology, Palaeoecology*, **421**, 24–47.
- Cantalejo, B., Pickering, K.T., McNiocail, C., Bown, P., Johansen, K. and Grant, M. 2020. A revised age-model for the Eocene deep-marine siliciclastic systems, Aínsa Basin, Spanish Pyrenees. Geological Society of London, *in press*.
- Carvajal, C., Steel, R. and Petter, A. 2009. Sediment supply: The main driver of shelf-margin growth. *Earth-Science Reviews*, **96**, 221–248.
- Castelltort, S., Honegger, L., Adatte, T., Clark, J.D., Puigdefàbregas, C., Spangenberg, J.E., Dykstra, M.L. and Fildani, A. 2017. Detecting climatic and tectonic signals with carbon isotopes in deep-marine strata, Eocene Aínsa basin, Spanish Pyrenees. *Geology*, **45**, 707–710.
- Cecil, C.B. 2013. An overview and interpretation of autocyclic and allocyclic processes and the accumulation of strata during the Pennsylvanian-Permian transition in the central Appalachian Basin, USA. *International Journal of Coal Geology*, **119**, 21–31.
- Clarke, L., Quine, T.A. and Nicholas, A. 2010. An experimental investigation of autogenic behaviour during alluvial fan evolution. *Geomorphology*, **115**, 278–285.

- Clevis, Q., de Boer, P. and Wachter, M. 2003. Numerical modelling of drainage basin evolution and three-dimensional alluvial fan stratigraphy. *Sedimentary Geology*, **163**, 85–110.
- Costa, E., Garcés, M., López-Blanco, M., Serra-Kiel, J., Bernaola, G., Cabrera, L. and Beamud, E. 2013. The Bartonian-Priabonian marine record of the eastern South Pyrenean Foreland Basin (NE Spain): A new calibration of the larger foraminifers and calcareous nannofossil biozonation, *Geologica Acta*, **11**, 177–193.
- Covault, J.A., Romans, B.W., Fildani, A., McGann, M. and Graham, S.A. 2010. Rapid Climatic Signal Propagation from Source to Sink in a Southern California Sediment-Routing System. *The Journal of Geology*, **118**, 247–259.
- Covault, J.A. and Graham, S. 2010. Submarine fans at all sea-level stands: Tectono-morphologic and climatic controls on terrigenous sediment delivery to the deep sea. *Geology*, **38**, 939–942.
- Covault, J., Normark, W., Romans, B. and Graham, S. 2007. Highstand fans in the California borderland: The overlooked deep-water depositional systems. *Geology*, **35**, 783–786.
- Damuth, J.E., Flood, R.D., Kowsmann, R.O., Belderson, R.H. and Gorini, M.A. 1988. Anatomy and growth pattern of Amazon deep-sea fan as revealed by long-range side-scan sonar (GLORIA) and high-resolution seismic studies. *American Association of Petroleum Geologists Bulletin*, **72**, 885–911.
- Das Gupta, K. 2008. *Tectono-stratigraphic evolution of deep-marine clastic systems in the Eocene Aínsa and Jaca basins, Spanish Pyrenees: petrographic and geochemical constraints*. University College London, 236 p.
- Das Gupta, K. and Pickering, K.T. 2008. Petrography and temporal changes in petrofacies of deep-marine Aínsa-Jaca basin sandstone systems, Early and Middle Eocene, Spanish Pyrenees. *Sedimentology*, **55**, 1083–1114.
- De Boer, P.L., Pragt, J.S.J. and Oost, A.P. 1991. Vertically persistent sedimentary facies boundaries along growth anticlines in the thrust-sheet-top South Pyrenean Tremp-Graus foreland basin. *Basin Research*, **3**, 63–78.

- DeConto, R.M. and Pollard, P. 2003. Rapid Cenozoic glaciation of Antarctica induced by declining atmospheric CO₂. *Nature*, **421**, 245–249.
- Deptuck, M.E., Piper, D.J.W., Savoye, B. and Gervais, A. 2008. Dimensions and architecture of late Pleistocene submarine lobes off the northern margin of East Corsica. *Sedimentology*, **55**, 869–898.
- Dinarés-Turell, J., Baceta, J.I., Pujalte, V., Orue-Etxebarria, X., Bernaola, G. and Lorito, S. 2003. Untangling the Palaeocene climatic rhythm: an astronomically calibrated Early Palaeocene magnetostratigraphy and biostratigraphy at Zumaia (Basque basin, northern Spain). *Earth and Planetary Science Letters*, **216**, 483–500.
- Dreyer, T., Corregidor, J., Arbués, P. and Puigdefábregas, C. 1999. Architecture of the tectonically influenced Sobrarbe deltaic complex in the Aínsa Basin, northern Spain. *Sedimentary Geology*, **127**, 127–169.
- Ducassou, E., Migeon, S., Mulder, T., Murat, A., Capotondi, L., Bernasconi, S.M. and Mascle, J. 2009. Evolution of the Nile deep-sea turbidite system during the Late Quaternary; influence of climate change on fan sedimentation. *Sedimentology*, **56**, 2061–2090.
- Dunne, L.A. and Hempton, M.R. 1984. Deltaic sedimentation in the Lake Hazar pull-apart basin, southeastern Turkey. *Sedimentology*, **31**, 401–412.
- Farrell, S.G., Williams, D.G. and Atkinson, C.D. 1987. Constraints on the age of movement of the Montsech and Cotiella Thrusts, south central Pyrenees, Spain. *Journal of the Geological Society, London*, **144**, 907–914.
- Feeley, M.H., Moore Jr.T.C., Loutit, T.S. and Bryant, W.R. 1990. Sequence stratigraphy of Mississippi Fan related to oxygen isotope sea level index. *American Association of Petroleum Geologists Bulletin*, **74**, 407–424.
- Fernández, O., Muñoz, J.A., Arbués, P., Falivene, O. and Marzo, M. 2004. 3-D reconstruction of geological surfaces: an example of growth strata and turbidite systems from the Aínsa basin (Pyrenees, Spain). *American Association of Petroleum Geologists Bulletin*, **88**, 1049–1068.

Fernández, O., Muñoz, J.A., Arbués, P. and Falivene, O. 2012. 3D structure and evolution of an oblique system of relaying folds: the Aínsa basin (Spanish Pyrenees). *Journal of the Geological Society London*, **169**, 545–559.

Flood, R.D. and Piper, D.J.W. 1997. Amazon Fan sedimentation: the relationship to equatorial climate change, continental denudation, and sea-level fluctuations. *In*: Flood, R.D., Piper, D.J.W., Klaus, A. and Peterson, L.C. (eds). *Proceedings of the Ocean Drilling Program, Scientific Results*, **155**, 653–675.

Flood, R.D., Manley, P.L., Kowsmann, R.O., Appi, C.J. and Pirmez, C. 1991. Seismic facies and late Quaternary growth of Amazon submarine fan. *In*: Weimer, P. and Link, M.H. (eds), *Seismic facies and sedimentary processes of modern and ancient submarine fans*, 415–433. New York, Springer-Verlag.

Gale, A.S., Young, J.R., Shackleton, N.J., Crowhurst, S.J. and Wray, D.S. 1999. Orbital tuning of Cenomanian marly chalk successions: towards a Milankovitch time-scale for the Late Cretaceous. *Philosophical transactions of the Royal Society of London*, **357**, 1815–1829.

Ganti, V., Straub, K.M., Foufoula-Georgiou, E. and Paola, C. 2011. Space-time dynamics of depositional systems: Experimental evidence and theoretical modeling of heavy-tailed statistics. *Journal of Geophysical Research*, **116**, 2156–2202.

Gómez-Paccard, M., López-Blanco, M., Costa, E., Garcés, M., Beamud, E. and Larrasoaña, J.C. 2011. Tectonic and climatic controls on the sequential arrangement of an alluvial fan/fan-delta complex (Montserrat, Eocene, Ebro Basin, NE Spain). *Basin Research*, **23**, 1–19.

Gradstein, F.M., Ogg, J.G. and Schmitz, M. 2012. *The Geological Time scale 2012*. Elsevier Science and Technology Books, Amsterdam.

Guillocheau, F. 2010. Control of alluvial sedimentation at foreland-basin active margins: A case study from the northeastern Ebro basin (southeastern Pyrenees, Spain). *Journal of Sedimentary Research*, **80**, 728–749.

Haq, B.U., Hardenbol, J. and Vail, P.R. 1987. Chronology of fluctuating sea levels since the Triassic (250 million years ago to present). *Science*, **235**, 1156–1167.

- Hays, J.D., Imbrie, I. and Shackleton, N.J. 1976. Variations in the Earth's orbit: pacemaker of the ice ages. *Science*, **194**, 1121–1132.
- Heard, T., Pickering, K.T. and Robinson, S.A. 2008. Milankovitch forcing of bioturbation intensity in deep-marine thin-bedded siliciclastic turbidites. *Earth and Planetary Science Letters*, **272**, 130–138.
- Holbourn, A., Kuhnt, W., Schulz, M. and Erlenkeuser, H. 2005. Impacts of orbital forcing and atmospheric carbon dioxide on Miocene ice-sheet expansion. *Nature*, **438**, 483–487.
- Holl, J.E. and Anastasio, D.J. 1993. Paleomagnetically derived folding rates, southern Pyrenees, Spain. *Geology*, **21**, 271–274.
- Horton, D.E., Poulson, C.J., Montañez, I.P. and DiMichele, W.A. 2012. Eccentricity-paced late Paleozoic climate change. *Palaeogeography, Palaeoclimatology, Palaeoecology*, **331–332**, 150–161.
- Huyghe, D., Castelltort, S., Mouthereau, F., Serra-Kiel, J., Filleaudeau, P., Emmanuel, L., Berthier, B. and Renard, M. 2012. Large scale facies change in the middle Eocene South-Pyrenean foreland basin: the role of tectonics and prelude to Cenozoic ice ages. *Sedimentary Geology*, **253–254**, 25–46.
- Imbrie, J., Hays, J.D., Martinson, D.G., McIntyre, A., Morley, J.J., Pisias, N.G., Prell, W.L. and Shackleton, N.J. 1984. The orbital theory of Pleistocene climate: support from a revised chronology of the marine $\delta^{18}\text{O}$ record. In: Berger, A.L., Imbrie, J., Hays, J., Kukla, G. and Saltzman, B. (eds), *Milankovitch and climate, Part 1*, 269–305. D Reidel, Hinham, MA, USA.
- Jorry, S.J., Jégou, I., Emmanuel, L., Silva Jacinto, R. and Savoye, B. 2011. Turbiditic levée deposition in response to climate changes: The Var Sedimentary Ridge (Ligurian Sea). *Marine Geology*, **279**, 148–161.
- Kemp, S.J., Ellis, M.A., Mounteney, I. and Kender, S. 2016. Palaeoclimatic implications of high resolution clay mineral assemblages preceding and across the onset of the Palaeocene–Eocene Thermal Maximum, North Sea Basin. *Clay Minerals*, **51**, 793–813.
- Kender, S., Stephenson M., Riding, J., Leng, M., O'B Knox, R., Peck V., Kendrick, C., Ellis, M., Vane, C. and Jamieson, R. 2012. Marine and terrestrial environmental changes in NW

Europe preceding carbon release at the Paleocene–Eocene transition. *Earth and Planetary Science Letters*, **353–354**, 108–120.

Kenyon, N.H., Amir, A. and Cramp, A. 1995. Geometry of the younger sediment bodies of the Indus Fan. *In*: Pickering, K.T., Hiscott, R.N., Kenyon, N.H., Ricci Lucchi, F. and Smith, R.D.A. (eds), *Atlas of Deep Water Environments: Architectural Style in Turbidite Systems*, 89–93. Chapman and Hall, London.

Kodama, K.P., Anastasio, D.J., Newton, M.L., Pares, J.M. and Hinnov, L.A. 2010. High-resolution rock magnetic cyclostratigraphy in an Eocene flysch, Spanish Pyrenees. *Geochemistry, Geophysics, Geosystems*, **11**, Q0AA07.

Kolla, V. and Coumes, F. 1987. Morphology, internal structure, seismic stratigraphy, and sedimentation on the Indus Fan. *American Association of Petroleum Geologists Bulletin*, **71**, 650–677.

Kolla, V. and Macurda Jr., D.B. 1988. Sea-level changes and timing of turbidity-current events in deep-sea fan systems. *In*: Wilgus, C.K., Hastings, B.K., Posamentier, H., Van Wagoner, J., Ross, C.A. and Kendall, C.G.St.C. (eds), *Sea-level changes: An Integrated Approach*, 381–392. Society of Economic Palaeontologists and Mineralogists Special Publication, **42**.

Kolla, V. and Perlmutter, M.A. 1993. Timing of turbidite sedimentation on the Mississippi Fan. *American Association of Petroleum Geologists Bulletin*, **77**, 1129–1141.

Kominz, M.A., Browning, J.V., Miller, K.G., Sugarman, P.J., Mizintseva, S. and Scotese, C.R. 2008. Late Cretaceous to Miocene sea-level estimates from the New Jersey and Delaware coastal plain coreholes: an error analysis. *Basin Research*, **20**, 211–226.

Kuehl, S.A., Hariu, T.M. and Moore, W.S. 1989. Shelf sedimentation off the Ganges-Brahmaputra river system: Evidence for sediment bypassing to the Bengal fan. *Geology*, **17**, 1132–1135.

Laskar, J., Fiengal, A., Gastineau, M. and Manche, H. 2011. La2010: a new orbital solution for the long-term motion of the Earth. *Astronomy and Astrophysics*, **532**, A89, 1–15.

- Lee, H.-K. and Schwarcz, H.P. 1996. Electron spin resonance plateau dating of periodicity of activity on the San Gabriel fault zone, southern California. *Geological Society of America Bulletin*, **108**, 735–746.
- Leon-Rodriguez, L. and Dickens, G.R. 2010. Constraints on ocean acidification associated with rapid and massive carbon injections: The early Paleogene record at ocean drilling program Site 1215, equatorial Pacific Ocean. *Palaeogeography, Palaeoclimatology, Palaeoecology*, **298**, 409–420.
- Li, Q., Gasparini, N.M. and Straub, K.M. 2018. Some signals are not the same as they appear: How do erosional landscapes transform tectonic history into sediment flux records? *Geology*, **46**, 407–410.
- Liebrand, D. Lourens, L.J., Hodell, D.A., de Boer, B., van de Wal, R.S.W. and Pälike, H. 2011. Antarctic ice sheet and oceanographic response to eccentricity forcing during the early Miocene. *Climates of the Past*, **7**, 869–880.
- López-Blanco, M., M. Marzo and J.A. Muñoz 2003. Low-amplitude, synsedimentary folding of a deltaic complex: Roda sandstone (lower Eocene), South-Pyrenean Foreland *Basin, Basin Research*, **15**, 73–95.
- Lourens, L.J., Sluijs, A., Kroon, D., Zachos, J. C., Thomas, E., Rohl, U., Bowles, J. and Raffi, I. 2005. Astronomical pacing of late Palaeocene to early Eocene global warming events. *Nature*, **435**, 1083–1087.
- Ma, W.T., Tian, J., Li, Q.Y. and Wang, P.X. 2011. Simulation of long eccentricity (400-kyr) cycle in ocean carbon reservoir during Miocene climate optimum: Weathering and nutrient response to orbital change. *Geophysical Research Letters*, **38**, L10701
doi:10.1029/2011GL047680
- Maldonado, A. and Stanley, D.J.W. 1976. The Nile Cone: submarine fan development by cyclic sedimentation. *Marine Geology*, **20**, 27–40.
- Manley, P.L. and Flood, R.D. 1988. Cyclic sediment deposition within Amazon deep-sea fan. *American Association of Petroleum Geologists Bulletin*, **72**, 912–925.

- Martinez-Braceras, N., Payros, A., Miniati, F., Arostegi, J. and Franceschetti, G. 2017. Contrasting environmental effects of astronomically driven climate change on three Eocene hemipelagic successions from the Basque–Cantabrian Basin. *Sedimentology*, **64**, 960–986.
- Martinsen, O.J. and Bakken, B. 1990. Extensional and compressional zones in slumps and slides in the Namurian of County Clare, Ireland. *Journal of the Geological Society*, **147**, 153–164.
- Marz, C., Hoffmann, J., Bleil, U., de Lange, G.J. and Kasten, S. 2008. Diagenetic changes of magnetic and geochemical signals by anaerobic methane oxidation in sediments of the Zambezi deep-sea fan (SW Indian Ocean). *Marine Geology*, **255**, 118–130.
- Marzo, M., Nijman, W. and Puigdefábregas, C. 1988. Architecture of the Castissent fluvial sheet sst, Eocene, Southern Pyrenees, Spain. *Sedimentology*, **35**, 719–738.
- Maslin, M., Knutz, P.C. and Ramsay, T. 2006. Millennial-scale sea-level control on avulsion events on the Amazon Fan. *Quaternary Science Reviews*, **25**, 3338–3345.
- McHargue, T.R. 1991. Seismic facies, processes, and evolution of Miocene inner fan channels, Indus Submarine Fan. In: Weimer, P. and Link, M.H. (eds), *Seismic Facies and Sedimentary Processes of Submarine Fans and Turbidite Systems*, 403–413. Springer, New York.
- Miller, K.G. and Wright, J.D. 2017. Success and failure in Cenozoic global correlations using golden spikes: a geochemical and magnetostratigraphic perspective. *Episodes*, **40**, doi.org/10.18814/epiiugs/2017/v40i1/017003
- Miller, K.G., Kominz, M.A., Browning, J.V., Wright, J.W., Mountain, G.S., Katz, M.E., Sugarman, P.J., Cramer, B.S., Christie-Blick, N. and Pekar, S.F. 2005. The Phanerozoic record of global sea-level change. *Science*, **310**, 1293–1298.
- Milliman, J.D. and Syvitski, J.P.M. 1992. Geomorphic/tectonic control of sediment discharge to the ocean: the importance of small mountainous rivers. *Journal of Geology*, **100**, 525–544.
- Millington, J.J. and Clark, J.D. 1995. The Charo/Arro canyon-mouth sheet system, south-central Pyrenees, Spain: a structurally influenced zone of sediment dispersal. *Journal of Sedimentary Research*, **65**, 443–454.

- Mochales, T., A. Barnolas, E.L. Pueyo, J. Serra-Kiel, A.M. Casas, J.M. Samsó, J. Ramajo and J. Sanjuán 2012a. Chronostratigraphy of the Boltaña anticline and the Aínsa Basin (Southern Pyrenees). *Geological Society of American Bulletin*, **124**, 1229–1250.
- Mochales, T., Casas, A.M., Pueyo, E.L. and Barnolas, A. 2012b. Rotational velocity for oblique structures (Boltaña anticline, Southern Pyrenees). *Journal of Structural Geology*, **35**, 2–16.
- Moody, J., Pyles, D., Julian, C., Bouroullec, R. 2012. Quantitative outcrop characterization of an analog to weakly confined submarine channel systems: Morillo 1 member, Aínsa Basin, Spain. *American Association of Petroleum Geologists Bulletin*, **96**, 11813–1841.
- Morley, C.K., Vanhauwaert, P. and DeBatist, M. 2000. Evidence for high frequency cyclic fault activity from high resolution seismic reflection survey, Rukwa rift, Tanzania. *Journal of the Geological Society London*, **157**, 983–994.
- Mouslopoulou, V., Walsh, J.J. and Nicol, A. 2009. Fault displacement rates on a range of timescales. *Earth and Planetary Science Letters* **278**, 186–197.
- Muller, R.A. and MacDonald, G.J. 2000. Ice ages and astronomical causes. *Data, spectral analysis and mechanisms*, 19-40. Springer, Praxis Publishing, Chichester, UK.
- Muñoz, J.A., McClay, K. and Poblet, J. 1994. Synchronous extension and contraction in frontal thrust sheets of the Spanish Pyrenees. *Geology*, **22**, 921–924.
- Muñoz, J.A., Arbués, P. and Serra-Kiel, J. 1998. The Aínsa basin and the Sobrarbe oblique thrust system: sedimentological and tectonic processes controlling slope and platform sequences deposited synchronously with a submarine emergent thrust system. In: Meléndez Hevia, A. and Soria, A.R. (eds), *Field Trip Guidebook of the 15th International Association of Sedimentologists International Congress of Sedimentology*, 213–223. International Association of Sedimentologists.
- Muñoz, J.A., Beamud, E., Fernández, O., Arbués, P., Dinarès-Turell, J. and Poblet, J. 2013. The Aínsa fold and thrust oblique zone of the central Pyrenees: kinematics of a curved contractional system from paleomagnetic and structural data. *Tectonics*, **32**, 1142–1175.
- Mutti, E., Tinterri, R., Benevelli, G., DiBiase, D. and Cavanna, G. 2003. Deltaic, mixed and turbidite sedimentation of ancient foreland basins. In: Mutti, E., Steffens, G.S., Pirmez, C.,

Orlando, M. and Roberts, D. (eds), Turbidites: models and problems. *Marine and Petroleum Geology*, **20**, 733–755.

Mutti, E., Remacha, E., Sgavetti, M., Rosell, J., Valloni, R. and Zamorano, M. 1985. Stratigraphy and facies characteristics of the Eocene Hecho Group turbidite systems, south-central Pyrenees. In: Mila, M.D. and Rosell, J. (eds), *Excursion Guidebook of the 6th European Regional Meeting of International Association of Sedimentologists, Lerida*, 233–291. International Association of Sedimentologists.

Mutti, E. and Sonnino, M. 1981. Compensational cycles: a diagnostic feature of turbidite sandstone lobes. In: *International Association of Sedimentologists, Second European Regional Meeting*, 120–123. International Association of Sedimentologists.

Mutti, E., Luterbacher, H.P., Ferrer, J. and Rosell, J. 1972. Schema stratigrafico e lineamenti di facies del Paleogene marino della zona central subpirenaica tra Tremp (Catalogna) e Pamplona (Navarra). *Societa Geologica Italiana*, **11**, 391–416.

Mutti, E. 1983/1984. The Hecho Eocene Submarine Fan System, South-Central Pyrenees, Spain. *Geo-Marine Letters*, **3**, 199–202.

Nakajima, T. and Itaki, T. 2007. Late Quaternary terrestrial climatic variability recorded in deep-sea turbidites along the Toyama Deep-Sea Channel, central Japan Sea. *Palaeogeography, Palaeoclimatology, Palaeoecology*, **247**, 162–179.

Nelson, C.H., Twichell, D.C., Schwab, W.C., Lee, H.J. and Kenyon, N.H. 1992. Upper Pleistocene turbidite sand beds and chaotic silt beds in the channelized, distal, outer-fan lobes of the Mississippi Fan. *Geology*, **20**, 693–696.

Nicholas, A.P. and Quine, T.A. 2007. Modelling alluvial landform change in the absence of external environmental forcing. *Geology*, **35**, 527–530.

Nicol, A., Walsh, J., Watterson, J. and Underhill, J.R. 1997. Displacement rates of normal faults. *Nature*, **390**, 157–159.

Nicol, A., Walsh, J., Manzocchi, T. and Morewood, N. 2005. Displacement rates and average earthquake recurrence intervals on normal faults. *Journal of Structural Geology*, **27**, 541–551.

- Nijman, W. 1998. Cyclicity and basin axis shift in a piggyback basin: towards modelling of the Tresp-Ager Basin, South Pyrenees, Spain. *In*: Mascle, A., Puigdefabregas, C., Luterbacher, H.P. and Fernández, M. (eds), *Cenozoic Foreland Basins of Western Europe*, 135-162. Geological Society, London, Special Publication, **134**.
- Normark, W.R., Damuth, J.E., Cramp, A., Flood, R.D., Hiscott, R.N., Kowsmann, R.O., Lopez, M., Manley, P.L., Nanayama, F., Piper, D.J.W., Pirmez, C. and Schneider, R.R. 1997. Sedimentary facies and associated depositional elements of the Amazon Fan. *In*: Flood, R.D., Piper, D.J.W., Klaus, A., Burns, S.J., Busch, W.H., Cisowski, S.M., Cramp, A., Damuth, J.E., Goni, M.A., Haberle, S.G., Hall, F.R., Hinrichs, K., Hiscott, R.N., Kowsmann, R.O., Kronen, J.D., Long, D., Lopez, M., McDaniel, D.K., Manley, P., Maslin, M.A., Mikkelsen, N., Nanayama, F., Normark, W.R., Pirmez, C., dos Santos, J.R., Schneider, R.R., Showers, W.J., Soh, W., Thibaut, J. and Fox, G.L., *Proceedings of the Ocean Drilling Program, Scientific Results*, Ocean Drilling Program, College Station, **155**, 611–651.
- Paillard, D., Labeyrie, L. and Yiou, P. 1996. Macintosh program performs time-series analysis. *Eos, Transactions American Geophysical Union*, **77**, 379.
- Pälike, H., Frazier, J. and Zachos, J.C. 2006a. Extended orbitally forced palaeoclimatic records from the Equatorial Atlantic Ceara Rise. *Quaternary Science reviews*, **25**, 3138–3149.
- Pälike, H., Norris, R.D., Herrle, J.O., Wilson, P.A., Coxall, H.K., Lear, C.H., Shackleton, N.J., Tripathi, A.K. and Wade, B.S. 2006b. The heartbeat of the Oligocene climate system. *Science*, **314**, 1894–1898.
- Parsons, J.D., Schweller, W.J., Stelting, C.W., Southard, J.B., Lyons, W.J. and Grotzinger, J.P. 2002. A preliminary experimental study of turbidite fan deposits. *Journal of Sedimentary Research*, **72**, 619-628.
- Payros, A. and Martínez-Braceras, N. 2014. Orbital forcing in turbidite accumulation during the Eocene greenhouse interval. *Sedimentology*, **61**, 1411–1432.
- Payros, A., Tosquella, J., Bernaola, G., Dinarès-Turell, J., Orue-Etxebarria, X. and Pujalte, V. 2009. Filling the North European Early/Middle Eocene (Ypresian/Lutetian) boundary gap: Insights from the Pyrenean continental to deep-marine record. *Palaeogeography, Palaeoclimatology, Palaeoecology*, **280**, 313–332.

- Peper, T. and de Boer, P.L. 1995. Intrabasinal thrust-tectonic versus climate control on rhythmicities in the Eocene South Pyrenean Tresp-Graus foreland basin: inferences from forward modelling. *Tectonophysics*, **249**, 93–107.
- Peper, T., Beekman, F. and Cloetingh, S. 1992. Consequences of thrusting and intraplate stress fluctuations for vertical motions in foreland basins and peripheral areas. *Geophysical Journal International*, **111**, 104–126.
- Pickering, K.T. and Cantalejo, B. 2015. Deep-marine environments of the Middle Eocene Upper Hecho Group, Spanish Pyrenees: Introduction. *Earth-Science Reviews*, **144**, 1–9.
- Pickering, K.T. and Corregidor, J. 2005. Mass-Transport Complexes (MTCs) and tectonic control on basin-floor submarine fans, Middle Eocene, South Spanish Pyrenees. *Journal of Sedimentary Research*, **75**, 761–783.
- Pickering, K.T. and Hiscott, R.N. (with contribution from T. Heard) 2016. *Deep Marine Systems: Processes, Deposits, Environments, Tectonic and Sedimentation*. Wiley and American Geophysical Union (AGU), ISBN: 978-1-4051-2578-9, 672 p.
- Pickering, K.T. and Bayliss, N.J. 2009. Deconvolving tectono-climatic signals in deep-marine siliciclastics, Eocene Aínsa basin, Spanish Pyrenees: seesaw tectonics versus eustasy. *Geology*, **37**, 203–206.
- Pickering, K.T., Souter, C., Oba, T., Taira, A., Schaaf, M. and Platzman, E. 1999. Glacio-eustatic control on deep-marine clastic forearc sedimentation, Pliocene - mid-Pleistocene (c. 1180–600 ka) Kazusa Group, SE Japan. *Journal of the Geological Society, London*, **156**, 125–136.
- Piper, D.J.W. and Normark, W.R. 1983. Turbidite depositional patterns and flow characteristics, Navy submarine fan, California Borderland. *Sedimentology*, **30**, 681–694.
- Popescu, I., Lericolais, G., Panin, N., Wong, H.K. and Droz, L. 2001. Late Quaternary channel avulsions on the Danube deep-sea fan, Black Sea. *Marine Geology*, **179**, 25–37.
- Prélat, A., Covault, J.A., Hodgson, D.M., Fildani, A. and Flint, S.S. (2010) Intrinsic controls on the range of volumes, morphologies, and dimensions of submarine lobes. *Sedimentary Geology*, **232**, 66–76.

Prins, M.A., Postma, G., Cleveringa, J., Cramp, A. and Kenyon, N.H. 2000. Controls on terrigenous sediment supply to the Arabian Sea during the late Quaternary; the Indus Fan. *Marine Geology*, **169**, 327–349.

Puigdefábregas, C., Muñoz, J.A. and Marzo, M. 1986. Thrust belt development in the eastern Pyrenees and related depositional sequences in the southern foreland basin. *In*: Allen, P.A. and P. Homewood, P. (eds), *Foreland Basins*, 229–246. Special Publication of the International Association of Sedimentologists, **8**.

Puigdefábregas, C., Muñoz, J.A. and Vergés, J. 1992. Thrusting and foreland basin evolution in the Southern Pyrenees. *In*: McClay, K.R. (ed.), *Thrust Tectonics*, 247–254. Chapman and Hall.

Remacha, E. and Fernández, L.P. 2003. High-resolution correlation patterns in the turbidite systems of the Hecho Group (South-Central Pyrenees, Spain). *Marine and Petroleum Geology*, **20**, 711–726.

Remacha, E., Gual, G., Bolaño, F., Arcuri, M., Oms, O., Climent, F., Crumeyrolle, P., Fernández, L.P., Vicente, J.C. and Suárez, J. 2003. Sand-rich turbidite systems of the Hecho Group from slope to the basin plain: facies, stacking patterns, controlling factors and diagnostic features. *American Association of Petroleum Geologists, International Conference and Exhibition, Barcelona, Spain, September*, 21–24. Geological Field Trip no. **12**, South-Central Pyrenees.

Rodríguez-Pintó, A., Pueyo, E.L., Serra-Kiel, J., Samsó, J.M., Barnolas, A. and Pocoví, A. 2012. Lutetian magnetostratigraphic calibration of larger foraminifera zonation (SBZ) in the Southern Pyrenees: the Isuela section, *Palaeogeography, Palaeoclimatology, Palaeoecology*, **333-334**, 107–120.

Ross, W.C., Halliwell, B.A., May, J.A., Watts, D.E. and Syvitski, J.P.M. 1994. Slope readjustment: a new model for the development of submarine fans and aprons. *Geology*, **22**, 511–514.

Ruddiman, W.F. 2006. Orbital changes and climate. *Quaternary Science Reviews*, **25**, 3092–3112.

Sames, B., Wagreich, M., Wendler, J.E., Haq, B.U., Conrad, C.P., Melinte-Dobrinescu, M.C., Hug, X., Wendler, I., Wolfgring, E., Yilmazi, I.Ö. and Zorina, S.O. 2016. Review: short-term

sea-level changes in a greenhouse world - a view from the Cretaceous. *Palaeogeography. Palaeoclimatology. Palaeoecology*, **441**, 393–411.

Sames, B., Wagreich, M., Conrad, C.P. and Iqbal, S. 2020. Aquifer-eustasy as the main driver of short-term sea-level fluctuations during Cretaceous hothouse climate phases. *Geological Society Special Publications*, **498**, 9–38.

Scotchman, J.I., Pickering, K.T., Sutcliffe, C., Dakin, N. and Armstrong, E. 2015. Milankovitch cyclicity within the middle Eocene deep-marine Guaso System, Aínsa Basin, Spanish Pyrenees. *Earth-Science Reviews*, **144**, 107–122.

Serra-Kiel, J., Canudo, J.I., Dinarés, J., Molina, E., Ortiz, N., Pascual, J.O., Samsó, J.M. and Tosquella, J. 1994. Cronostratigrafía de los sedimentos marinos del Terciario inferior de la Cuenca de Graus-Tremp (Zona Central Surpirenaica). *Revista de la Sociedad Geológica de España*, **7**, 273–297.

Shackleton, N.J., Hagelberg, T.K. and Crowhurst, S.J. 1995. Evaluating the success of astronomical tuning: pitfalls for using coherence as a criterion for assessing pre-Pleistocene timescales. *Paleoceanography*, **10**, 693–697.

Shevenell, A.E., Kennett, J.P. and Lea, D.W. 2004. Middle Miocene southern ocean cooling and Antarctic cryosphere expansion. *Science*, **305**, 1766–1770.

Smith, M.E., Carroll, A.R. Scott, J.C. and Singer, B.S. 2014. Early Eocene carbon isotope excursions and landscape destabilization at eccentricity minima: Green River Formation of Wyoming. *Earth and Planetary Science Letters*, **403**, 393–406.

Straub, K.M., Paola, C., Mohrig, D., Wolinski, M.A. and George, T. 2009. Compensational stacking of channelized sedimentary deposits. *Journal of Sedimentary Research*, **79**, 673–688.

Sutcliffe, C. and Pickering, K.T. 2009. End-signature of deep-marine basin-fill, as a structurally confined low-gradient clastic slope: the middle Eocene Guaso System, south-central Spanish Pyrenees. *Sedimentology*, **56**, 1670–1689.

Tabor, C.R., Poulsen, C.J. and Pollard, D. 2014. Mending Milankovitch's theory: obliquity amplification by surface feedbacks. *Climate of the Past*, **10**, 41–50.

- Tian, J., Yang, M., Lyle, W., Wilkens, R. and Shackford, J.K. 2013. Obliquity and long eccentricity pacing of the Middle Miocene climate transition. *Geochemistry, Geophysics, Geosystems*, **14**, 1740–1755.
- Toucanne, S., Zaragosi, S., Bourillet, J.-F., Dennielou, B., Jorry, S.J., Jouet, G. and Cremer, M. 2012. External controls on turbidite sedimentation on the glacially-influenced Armorican margin (Bay of Biscay, western European margin). *Marine Geology*, **303-306**, 137–153.
- Tripathi, A. and Darby, D. 2018. Evidence for ephemeral middle Eocene to early Oligocene Greenland glacial ice and pan-Arctic sea ice. *Nature Communications*, doi: 10.1038/s41467-018-03180-5.
- Tucker, G.E. and Slingerland, R. 1996. Predicting sediment flux from fold and thrust belts. *Basin Research*, **8**, 329–349.
- Von Rad, U. and Tahir, M. 1997. Late Quaternary sedimentation on the outer Indus shelf and slope (Pakistan): evidence from high-resolution seismic data and coring. *Marine Geology*, **138**, 193–236.
- Wade, B.S. and Pälike, H. 2004. Oligocene climate dynamics. *Paleoceanography and Paleoclimatology*, **19**, PA4019, doi:10.1029/2004PA001042.
- Walsh, J.J., Nicol, A. and Childs, C. 2002. An alternative model for the growth of faults. *Journal of Structural Geology*, **24**, 1669–1675.
- Weber, M.E., Wiedicke, M.H., Kudrass, H.R., Hübscher, C. and Erlenkeuser, H. 1997. Active growth of the Bengal Fan during sea-level rise and highstand. *Geology*, **25**, 315–318.
- Weber, M.E., Wiedicke-Hombach, M., Kudrass, H.R. and Erlenkeuser, H. 2003. Bengal Fan sediment transport activity and response to climate forcing inferred from sediment physical properties. *Sedimentary Geology*, **155**, 361–381.
- Weedon, G.P. 2005. *Time-series analysis and cyclostratigraphy (examining stratigraphic records of environmental cycles)*, 81–214. Cambridge University Press.
- Weedon, G.P., Coe, A.L. and Gallois, R.W. 2004. Cyclostratigraphy, orbital tuning and inferred productivity for the type Kimmeridge clay (Late Jurassic), Southern England. *Journal of the Geological Society, London*, **161**, 655–666.

- Weimer, P. 1990. Sequence stratigraphy, facies geometries, and depositional history of the Mississippi Fan, Gulf of Mexico. *American Association of Petroleum Geologists Bulletin*, **74**, 425–453.
- Weltje, G.J. and De Boer, P.L. 1993. Astronomically induced paleoclimatic oscillations reflected in Pliocene turbidite deposits on Corfu (Greece): implications for the interpretation of higher order cyclicity in ancient turbidite systems. *Geology*, **21**, 307–310.
- Weltje, G.J., van Ansenwoude, S.O.K.J. and De Boer, P.L. 1996. High-frequency detrital signals in Eocene fan-delta sandstones of mixed parentage (South-Central Pyrenees, Spain): a reconstruction of chemical weathering in transit. *Journal of Sedimentary Research*, **66**, 119–131.
- Weimer, P. 1990. Sequence stratigraphy, facies geometries, and depositional history of the Mississippi Fan, Gulf of Mexico. *American Association of Petroleum Geologists Bulletin*, **74**, 425–453.
- Westerhold, T., Röhl, U., Pälike, H., Wilkens, R., Wilson, P.A. and Acton, G. 2013. Orbitally tuned time scale and astronomical forcing in the middle Eocene to early Oligocene, *Climate of the Past Discussions*, **9**, 6635–6682.
- Westerhold, T., Röhl, U., Donner, B., Frederichs, T., Kordesch, W.E C., Bohaty, S.M., Hodell, D.A., Laskar, J. and Zeebe, R.E. 2018. Late Lutetian Thermal Maximum – crossing a thermal threshold in Earth’s climate system? *Geochemistry, Geophysics, Geosystems*, **19**, 73–82.
- Zachos, J.C., Shackleton, N.J., Revenaugh, J.S., Pälike, H. and Flower, B.P. 2001b. Climate response to orbital forcing across the Oligocene-Miocene boundary. *Science*, **292**, 274–278.
- Zachos, J.C., Röhl, U., Schellenberg, S.A., Sluijs, A., Hodell, D.A., Kelly, D.C., Thomas, E., Nicolo, M., Raffi, I., Lourens, L.J., McCarres, H. and Kroon, D. 2005. Rapid acidification of the ocean during the Paleocene-Eocene thermal maximum. *Science*, **308**, 1611–1615.

Figure captions

Figure 1. Stratigraphy of the Aínsa Basin in the context of the Gavarnie thrust sheet, modified from Arbués *et al.* (1998), Fernández *et al.* (2004), Fernández *et al.* (2012), and Muñoz *et al.* (2013).. Lithostratigraphic units: Es = Escanilla; Bu = Buil; So, Sobrarbe; Gu =

Guara; Gr, Grustán; Pa = Pano; Cp = Capella; Pr = Perarrúa; Cm = Campanué; Cst = Castissent; SM = Santa Marina; Cg = Castigaleu; Ro = Roda; Yb = Yeba; Ri = Riguala; Me = Metils; Mi = Millaris; Al = Alveolina limestone. SV1- 2. Hecho Group deep-marine siliciclastic systems (= San Vicente Formation of Muñoz *et al.* (2013)). Horizons: O = Olsón; EL = Escanilla limestone; SB = Santa Bárbara; SP = San Pedro; SL = San Lino; M = Morillo limestone; A = Ascaso; LP = La Puebla. Thrust sheets: C = Cotiella; M = Montsec; PM = Peña Montañesa; B and G = Bielsa and Guarga; LF = La Fueba thrust system. Unconformities: AT = L'Atiart; CL = Charo-Lascorz. Litho- and chronostratigraphic information compiled from Bentham (1992), Bentham and Burbank (1996), Barnolas and Gil-Peña (2001), López-Blanco *et al.* (2003), Mochales *et al.* (2012b), Rodríguez-Pintó *et al.* (2012), and Serra-Kiel *et al.* (1994). Eocene time scale from Gradstein *et al.* (2012). SBZ biozones calibration to the time scale integrates data from Costa *et al.* (2013) and Rodríguez-Pintó *et al.* (2012). A prominent basin-wide m-scale black mudstone/claystone likely is the Late Lutetian Thermal Maximum (LLTM) dated at 41.52 Ma (*cf.* Westerhold *et al.*, 2018).

Figure 2. Idealised vertical complete succession of a submarine fan in the Aínsa Basin. There is a general fining-upwards trend. Typical sandy fan thickness is ~ 10–70 m. Non-deposition, erosional processes and the location of the submarine fan within the basin (e.g., lateral, axial) can result in incomplete successions where bases and tops may be absent. Modified after Pickering and Corregidor (2005) and Pickering and Bayliss (2009).

Figure 3. Geographical location of the gamma-ray logged sections in the Aínsa Basin. From Pickering and Cantalejo (2015). The LLTM section is ~15 km south of Guaso.

Figure 4. Orbital tuning of the Gerbe section. The filtered total-gamma records of the Gerbe section (a) have been matched to the eccentricity cycles of the La2010a orbital solution of Laskar *et al.* (2011) orbital solution (b) using 5 anchor points designated with an asterisk (*). The resultant tuned records (c) show the distortion of the original data.

Figure 5. Orbital tuning of the Labuerda section 2. The filtered total-gamma records of the Labuerda section 2 (a) have been matched to the eccentricity cycles of the La2010a orbital solution of Laskar *et al.* (2011) orbital solution (b) using 9 anchor points designated with an asterisk (*). The resultant tuned records (c) show the distortion of the original data. The C21n-C20r magnetic reversal dated at 45.72 Ma found at ~185 m height in the Labuerda section 2 has also been used as a control point. The resultant tuned records (c) show the distortion of the original data.

Figure 6. Orbital tuning of the Boltaña section. Filtered total-gamma records of the Boltaña section (a) have been matched to eccentricity cycles of the La2010a orbital solution of Laskar *et al.* (2011) (b) using 6 anchor points designated with an asterisk (*). The resultant tuned records (c) show the distortion of the original data. The resultant tuned records (c) show the distortion of the original data.

Figure 7. Orbital tuning of the Forcaz section. Filtered total-gamma records of the Forcaz section (a) have been matched to eccentricity cycles of the La2010a orbital solution of Laskar *et al.* (2011) (b) using 8 anchor points designated with an asterisk (*). The resultant tuned records (c) show that the original data has undergone more distortion in the interval between 60 and 90 m height. The resultant tuned records (c) show the distortion of the original data.

Figure 8. Orbital tuning of the Morillo section. Filtered total-gamma records of the Morillo section (a) have been matched to obliquity cycles of the La2010a orbital solution of Laskar *et al.* (2011) (b) using 10 anchor points designated with an asterisk (*). The resulted tuned records (c) show the distortion of the original data.

Figure 9. Spectral analysis using REDFIT of total-gamma records tuned to eccentricity. The tuned records show a general strengthening of the obliquity peak and precession cycles with an increase in confidence levels.

Figure 10. Summary of all tuned sections with eccentricity minima in the Aínsa Basin in the relation to the sandy submarine fans. Note that as these sections are all off-axis in the fine-grained deposits, the onset of sandy fan accumulation started at some time prior to that shown in these sections, i.e., at a stratigraphically lower point.

Figure 11. Field photograph of the ~3 m-thick dark mudstone unit (with underlying thinner subsidiary dark layers) located between the upper part of the Guaso System and the Sobrarbe deltaic system. See Figure 11 for detailed sedimentary log.

Figure 12. Total gamma, K and Th records measured from portable spectrometer. Sample interval 20 cm with sample readings of 3 min to improve accuracy. The dark bands are characterised by the highest total gamma and K values. The LLTM interval likely includes both prominent dark bans in the boxed area. The high K and Th values likely reflect decreased carbonate and, therefore, greater clay mineral abundance as proposed by Westerhold *et al.* (2018) from Atlantic cores.

Figure 13. Revised chronostratigraphy of the sediments of the Aínsa Basin using the tuned gamma ray log sections to build a more accurate chronostratigraphy. Note that as these sections are all off-axis in the fine-grained deposits, the onset of sandy fan accumulation started at some time prior to that shown in these sections, i.e., at a stratigraphically lower point. Where a “?” symbol is indicated, the exact stratigraphic location of the submarine fan has pinch out and cannot be fully resolved. The Arro System is tectonically deformed with an overturned fold limb and associated with several thrusts / shear zones. Eccentricity and obliquity curves from Laskar *et al.* (2011). High resolution sea-level curves (Miller, unpublished) with 5-point moving average smoothed curve.

Figure 14. Mediano Anticline growth rates modified after Holl and Anastasio (1993). The Mediano Anticline underwent three main periods of relatively rapid growth during the deposition of the Hecho Group SGF deposits in the Aínsa Basin.

Supplementary Materials

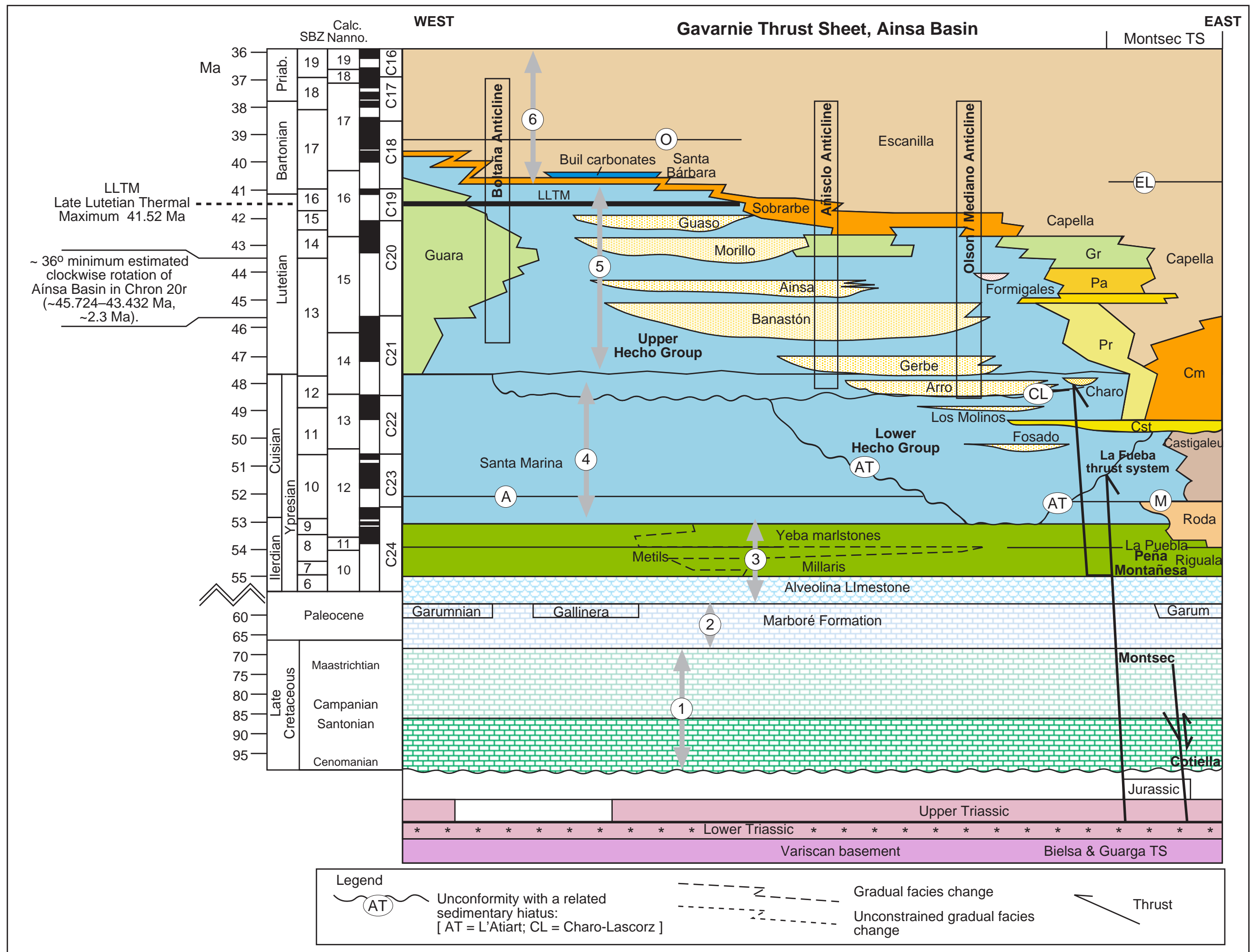
Supplementary material 1. The filtered records for each of the analysed gamma-ray logged sections. The filtered frequency has been associated with the short eccentricity cycle in Cantalejo & Pickering (2015).

Supplementary material 2. Anchor points used in the total natural gamma sections.

Supplementary material 3. SARs tables calculated for each of the tuned records.

Supplementary material 4. SARs graphs for all tuned gamma-ray sections.

Supplementary material 5. Alternative tuning for sections which lack radiometric control.



Facies

Sedimentary processes

Type Ia MTD



..... Storage of fluvial sands / gravels in non-marine and shallow marine settings.
Over steepened slope failure events

..... Denudation in hinterland to new equilibrium profile, submarine slope healing with reduction in sediment calibre and eventual fan abandonment

..... Channel infill/backfill

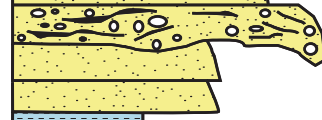
Type III MTD



..... Renewed channel incision and sediment bypass

..... Channel infill/backfill

Type III MTD



..... Renewed channel incision and sediment bypass

..... Channel infill/backfill

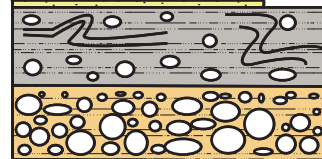
Type III MTD



..... Channel incision and sediment bypass

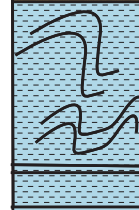
..... River-derived sandy turbidites (high % non-marine palynomorphs + woody material)

Type II MTD



..... Unconsolidated uppermost slope, shelf and littoral zone marine sands and gravels redeposited into deep water (+molluscan borings)

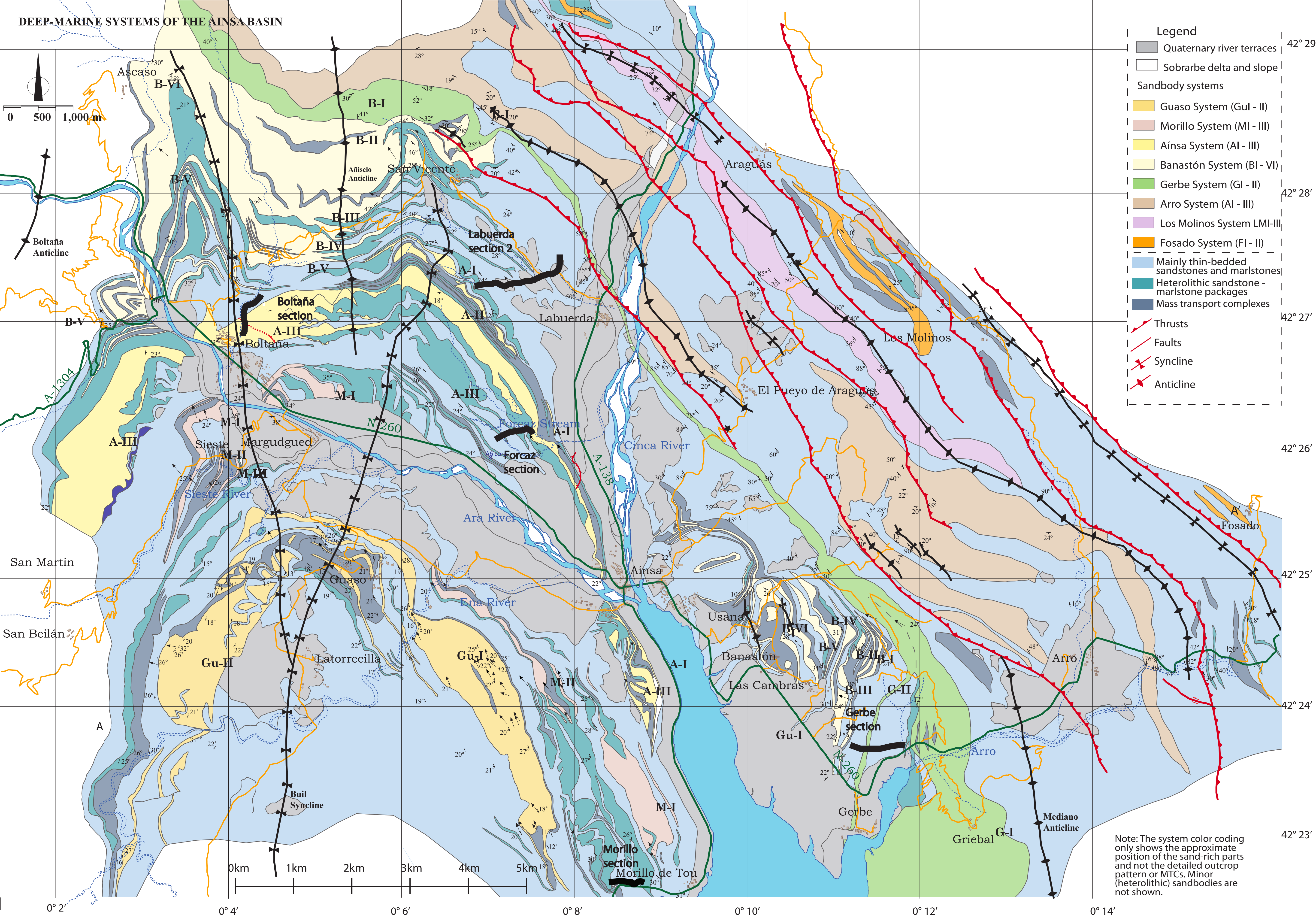
Type Ia MTD



..... Collapse of mid- to upper basin slope, redeposition of fine-grained sediments

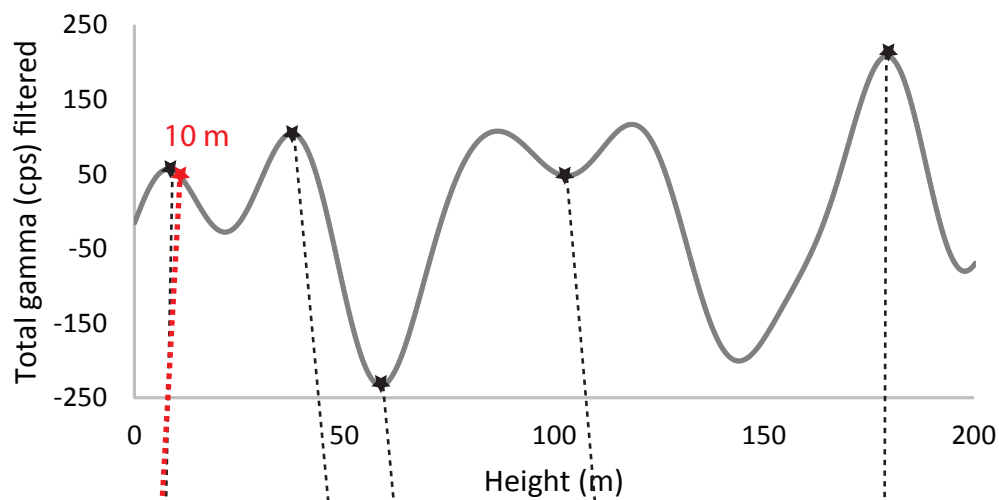
Individual channels show stepwise migration, erosion and infill (backfill) due to higher frequency poorly understood processes (including influence by local-intrabasinal growth structures)

DEEP-MARINE SYSTEMS OF THE AINSA BASIN

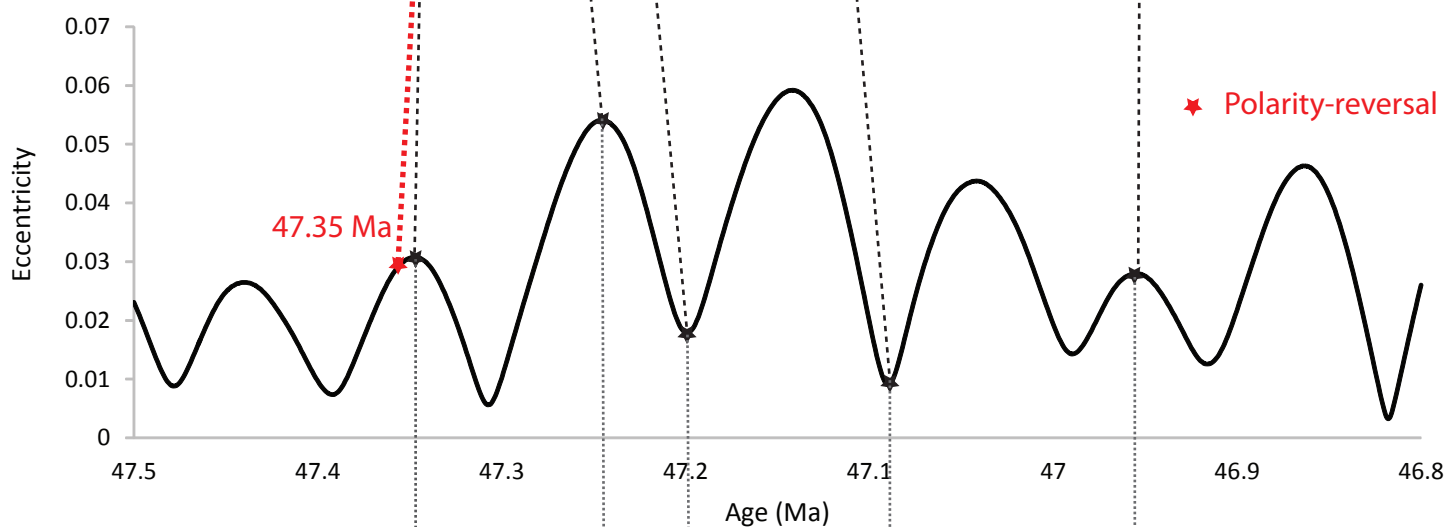


Note: The system color coding only shows the approximate position of the sand-rich parts and not the detailed outcrop pattern or MTCs. Minor (heterolithic) sandbodies are not shown.

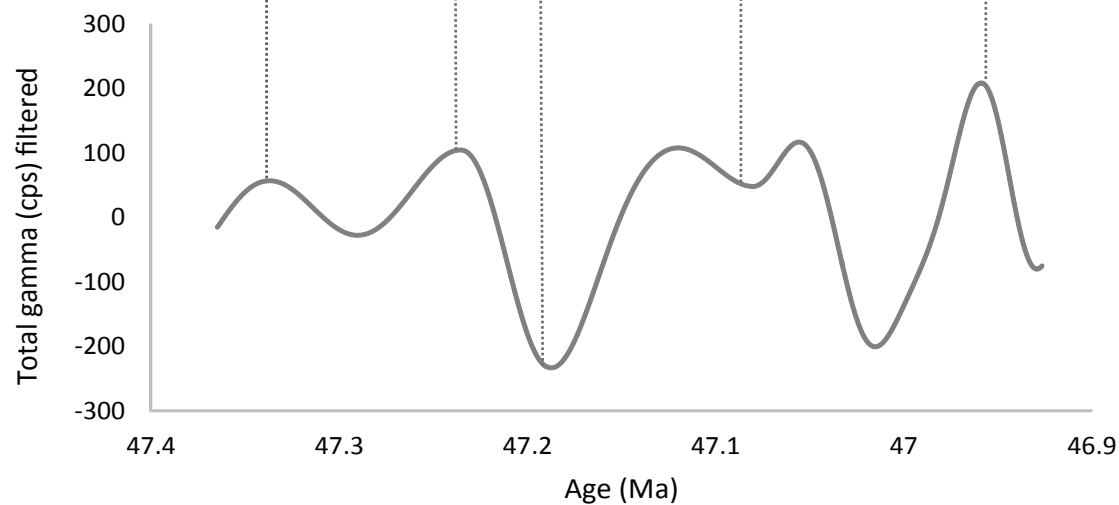
a)



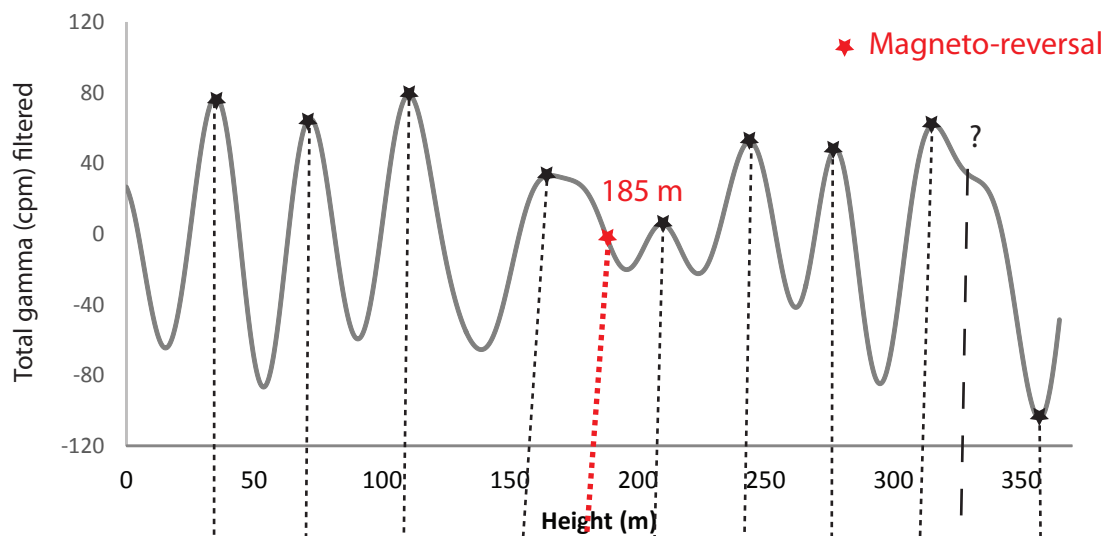
b)



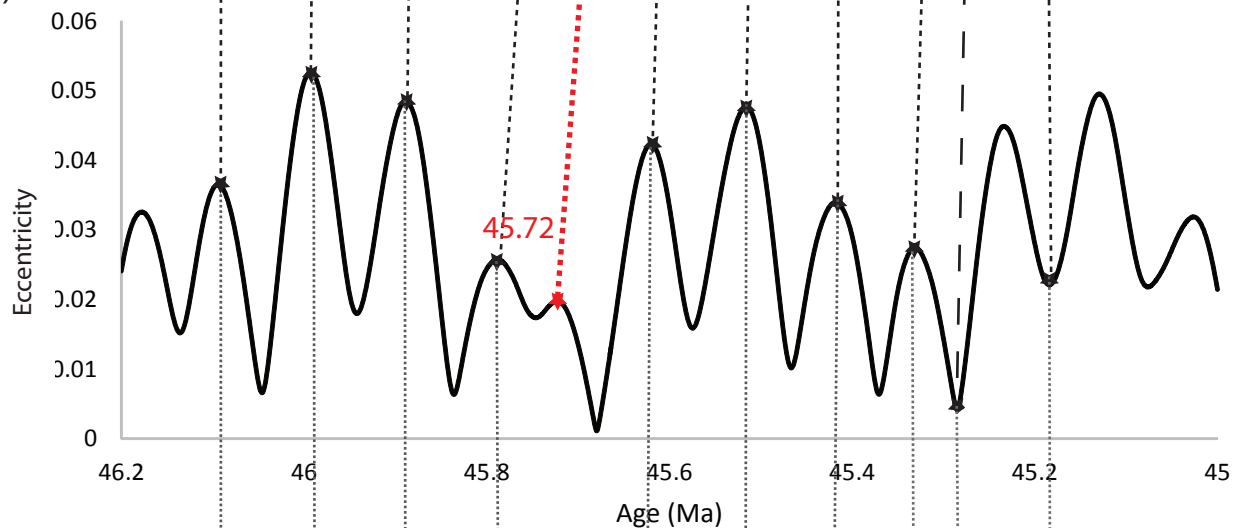
c)



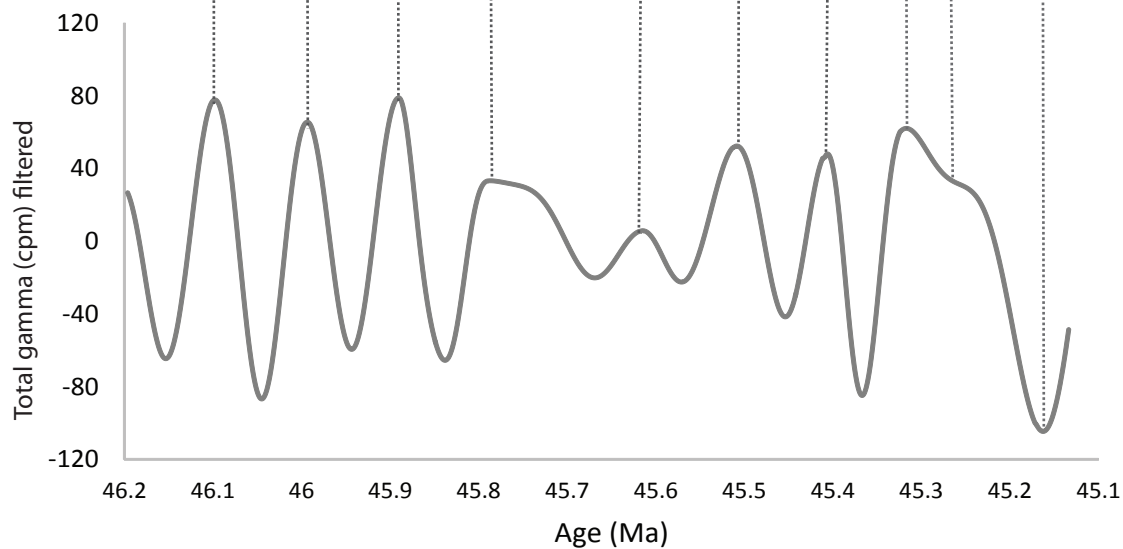
a)



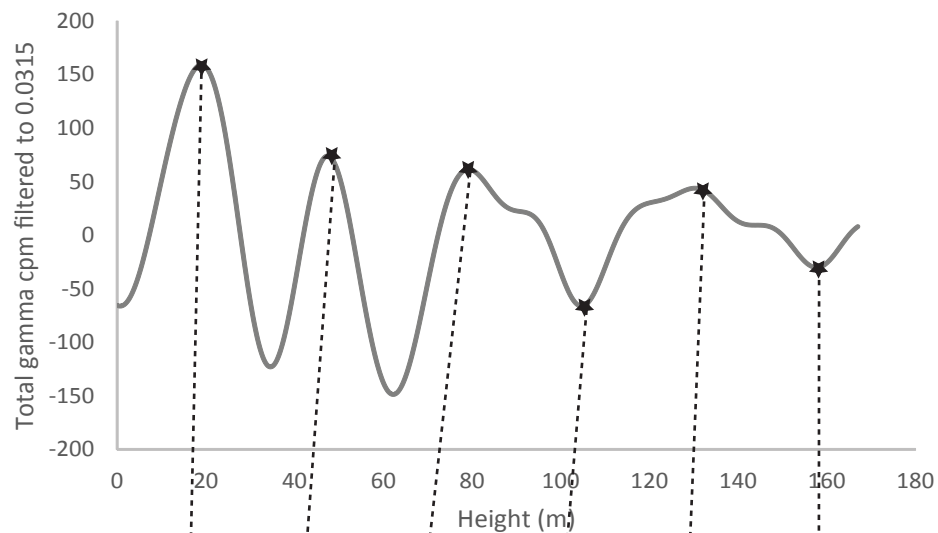
b)



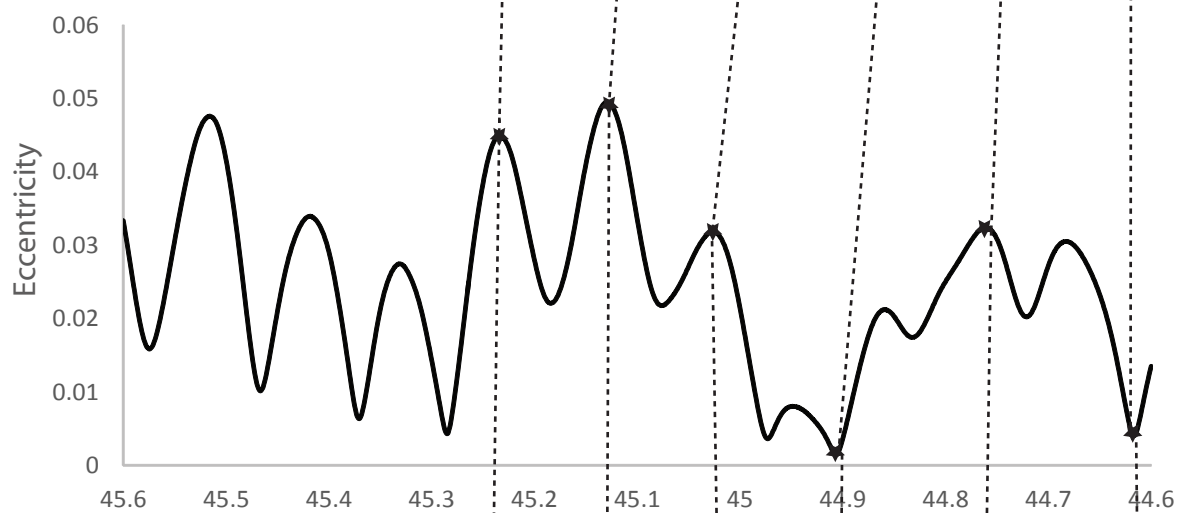
c)



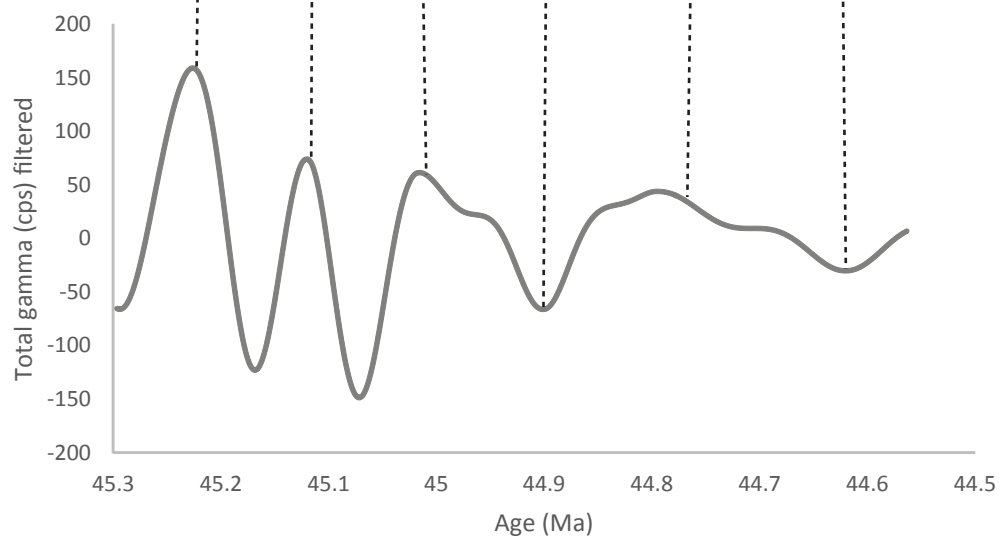
a)



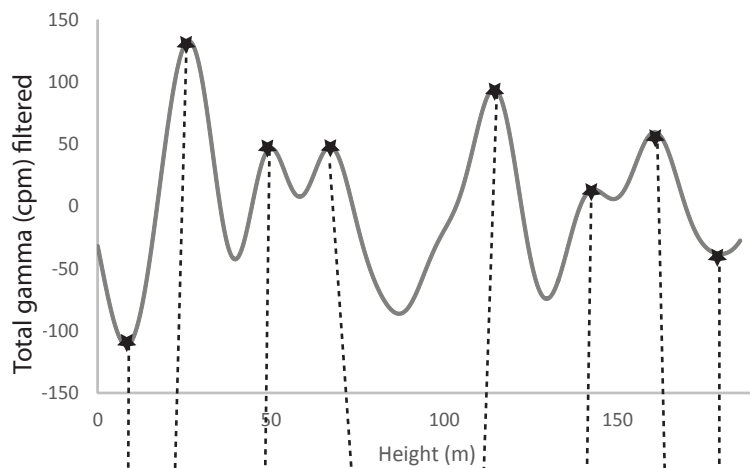
b)



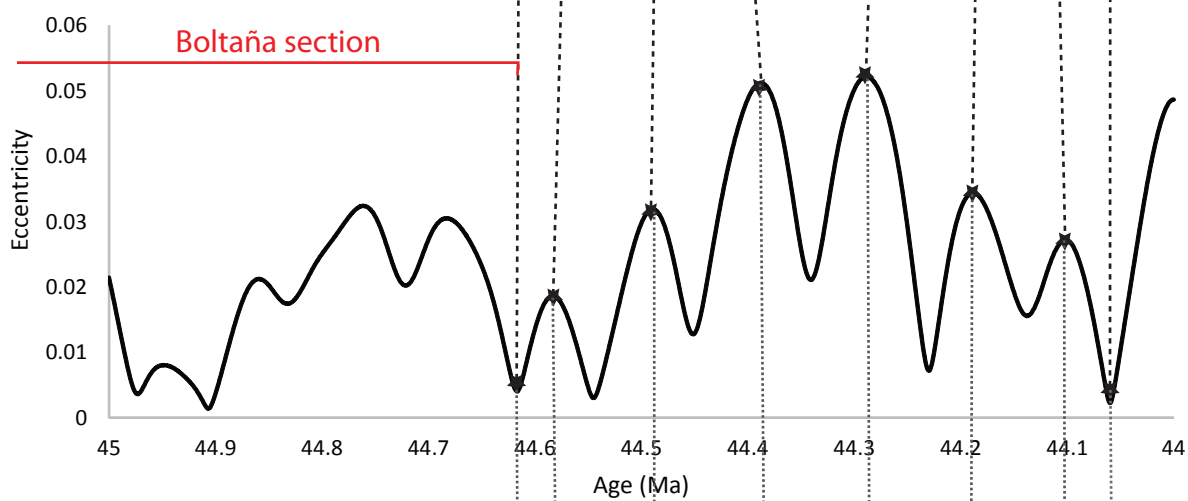
c)



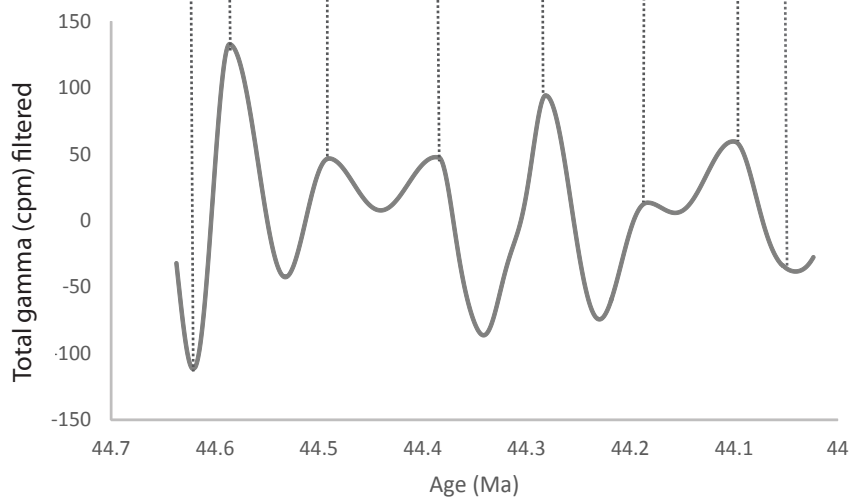
a)



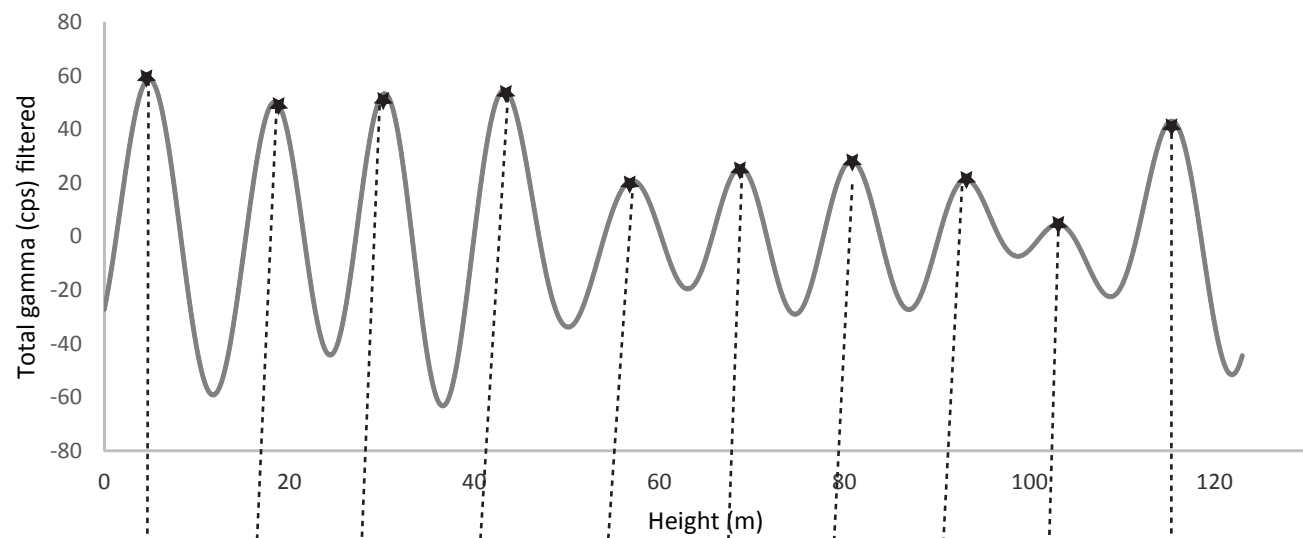
b)



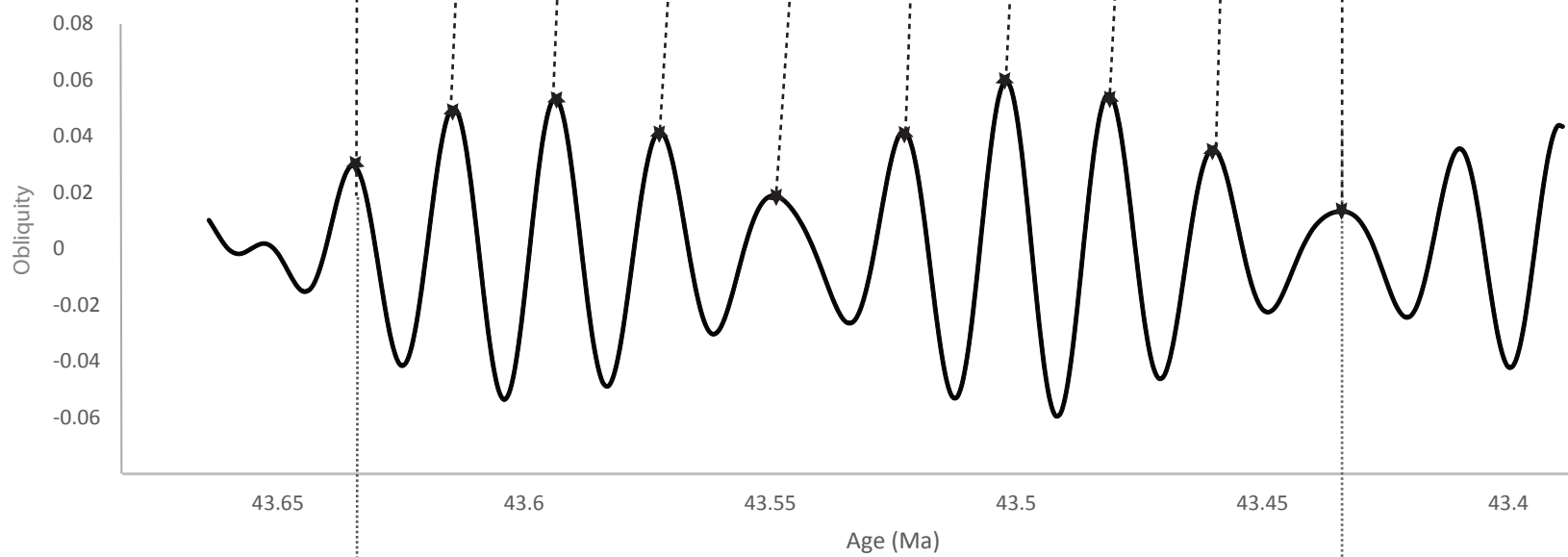
c)



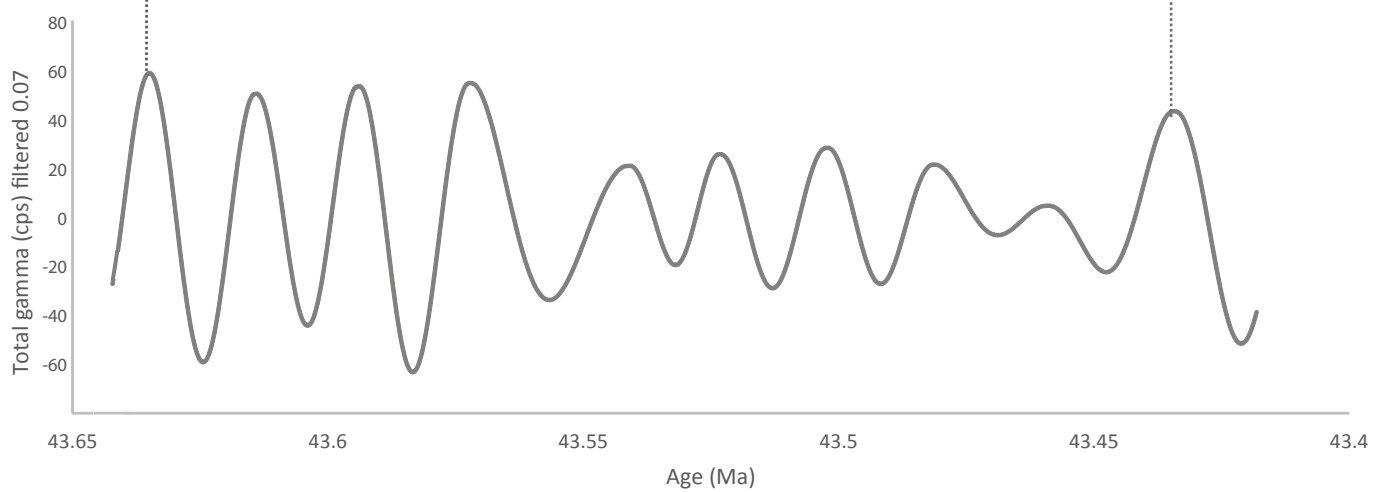
a)



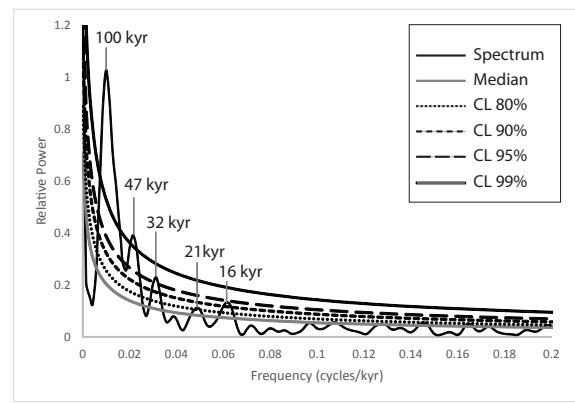
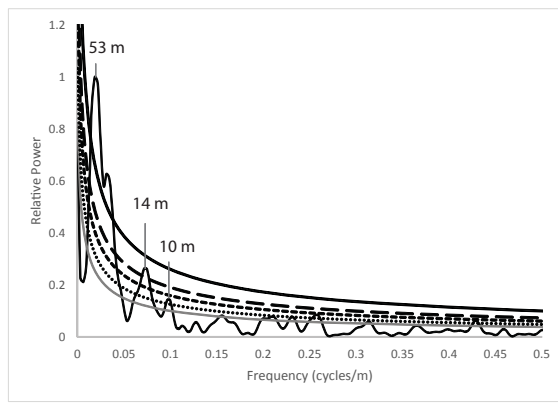
b)



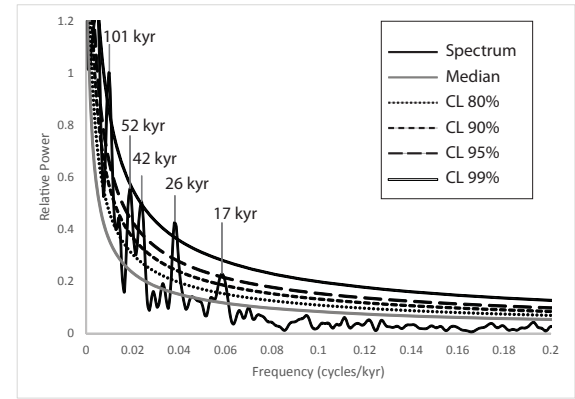
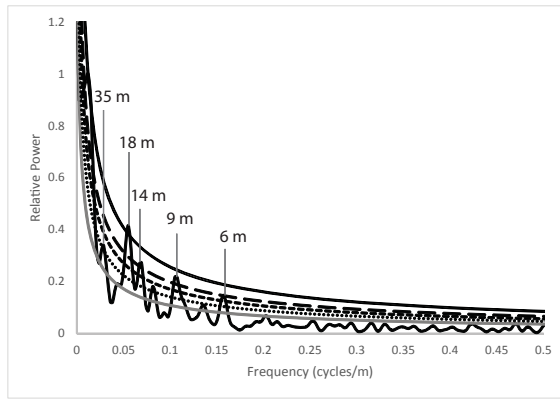
c)



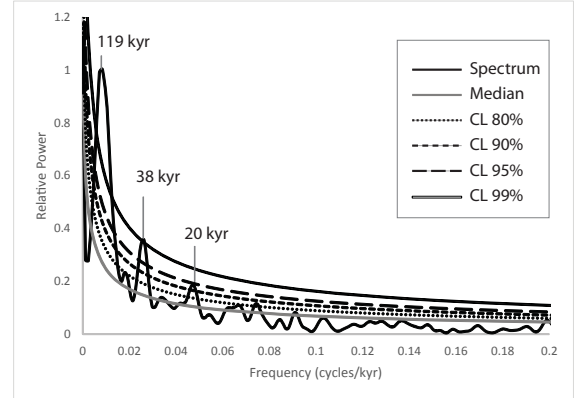
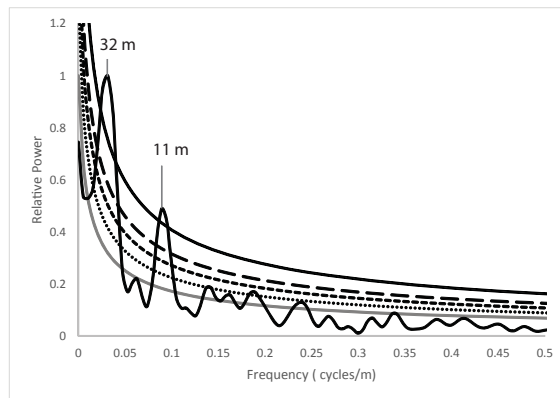
Gerbe section



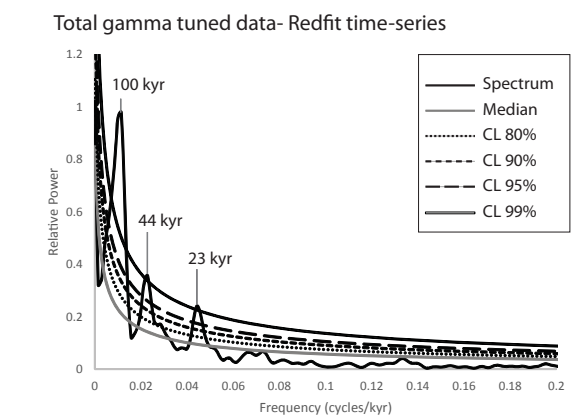
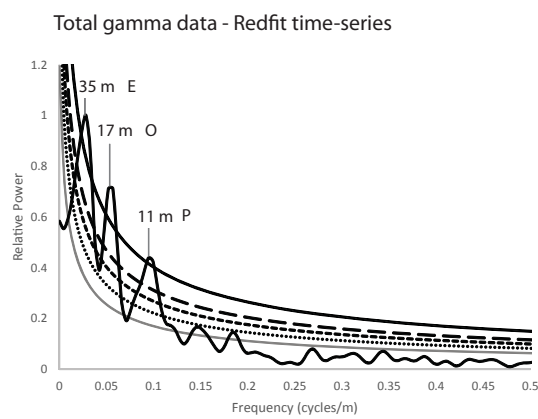
Labuerda section 2



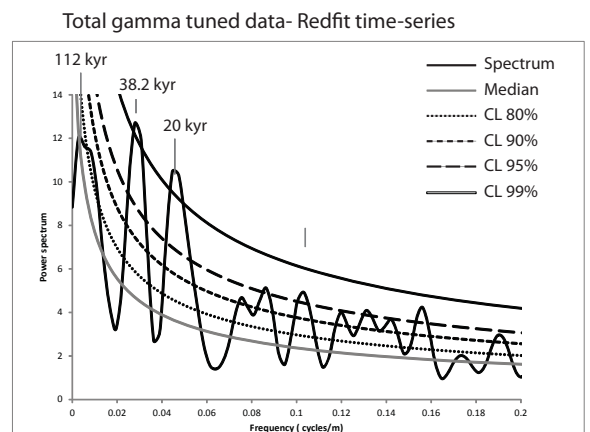
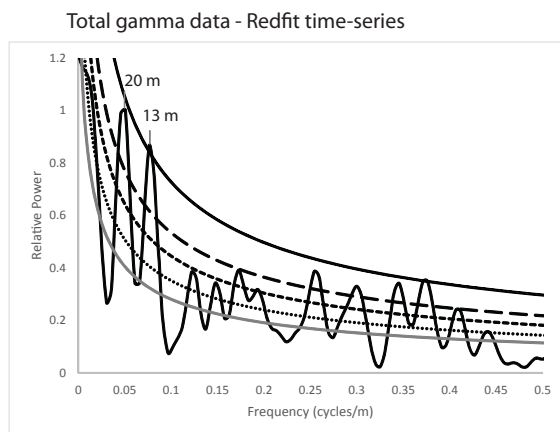
Boltaña section

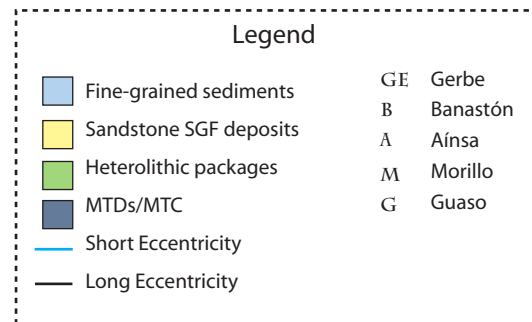
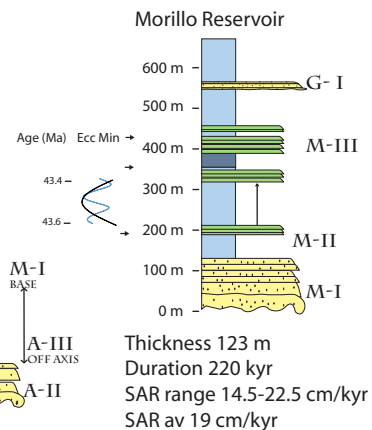
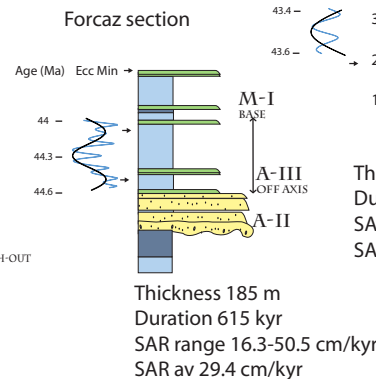
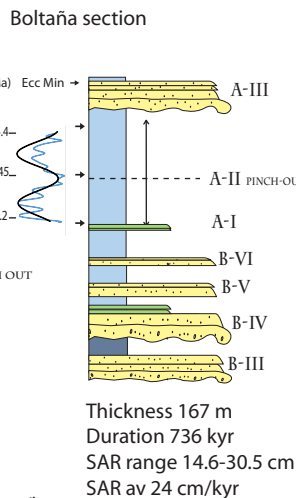
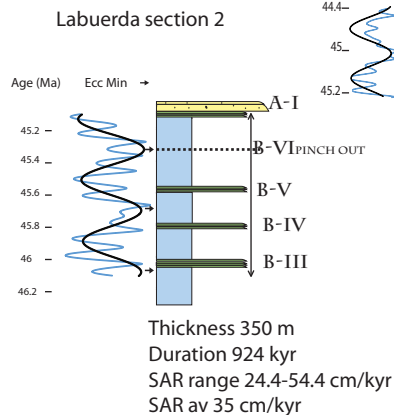
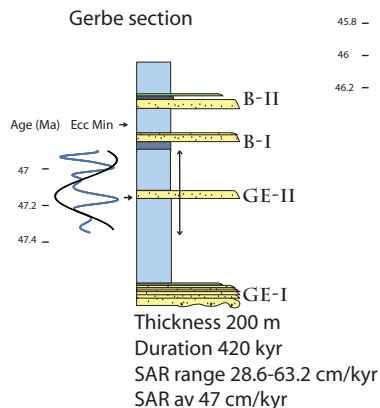


Forcaz section



Morillo section







Gamma-ray logged section

Dark band - peak LLTM

to Mondot →

← to road A 2205

Dark band - peak LLTM

